UNIVERSITY OF CALIFORNIA, SAN DIEGO

Physical Factors Affecting Larval Transport in Mission Bay, California

A thesis submitted in partial satisfaction of the requirements for the degree Master of Science

in

Engineering Sciences (Mechanical Engineering)

by

Erik Edwin Tang

Committee in charge:

Sarah Gille, Chair
Bruce Cornuelle
Kraig Winters

2010

The thesis of Erik Edwin Tang is approved and it is acceptable in quality and form for publication on microfilm and electronically:

_____

_____

_____

Chair

University of California, San Diego

2010

DEDICATION

First I would like to thank my mother and father, Louis and Kim Tang, for always supporting me in all my academic endeavors and always pushing me to perform to the best of my ability. If it were not for their encouragement and willingness to provide me all the tools needed to succeed, I would not be where I am today.

I would also like to thank my aunt, Muoi Tang, for motivating me to succeed in school at a young age. It was her positive feedback that motivated me to do well in school and always strive to do better.

Last but not least I would like to thank my two sisters, Ashley and Andrea, for continually supporting me and being there when I needed them. Andrea's strength and academic success has always served as a motivation for me to strive to be as successful as her. Ashley constantly reminds me that it is possible to be social and academically talented. Her ability to balance work, school, and a vivid social life has kept me well rounded and grounded.

To my 'brothers', HEDB, ladies and gents of S7, and CC, I want to thank all of you for providing some of the happiest memories in my life. Without you guys continually supporting me, making me laugh and being honest with me, I do not think I would have been able to achieve what I have, especially though the rough times. A bond between friends as strong as we have is not easily found, and I thank you all for allowing me to be a part of your lives.

Ms. Schrepferman was the first teacher to ever show me that I could have fun and learn a lot with academics. Due to her unique teaching style and willingness to always joke around with me in 8^{th} grade (Dog Years), she instilled a true passion in me for learning and improving my academic skills. I will never forget the fun times I had as a chubby 8^{th} grader in her class.

Mr. Harold Dorr introduced me to environmental science and engineering. His passion for the subject is clear in how he presented and talked about the material. His vast knowledge regarding oceanography along with his sense of humor made learning fun. He afforded me many opportunities and truly instilled in me a passion for the environment and ocean. Because of Mr. Dorr, I chose the path of an engineer.

TABLE OF CONTENTS

ACKNOWLEDGEMENTS

I would like to acknowledge Professor Sarah Gille for her support as the chair of my committee. Her continual aid and insight throughout this entire thesis process has taught me so much about the academic process and improved my skills as a researcher many fold. Her guidance has proved to be invaluable.

I would also like to acknowledge Julia Cornuelle, Bruce Cornuelle, Linda Rasmussen and Lisa Levin. Julia has introduced me to the world of hydrodynamic modeling which I would have never had the opportunity to experience if not for her. I would like to thank her for our countless meetings and the many hours she spent working with me. Bruce was a great resource to me when I had any questions or problems. He played a key role in setting up the hydrodynamic models and was a great help. Linda Rasmussen and Lisa Levin have provided much insight into the ecological and environmental significance of this work which has aided me throughout this study.

ABSTRACT OF THE THESIS

Physical Factors Affecting Larval Transport in Mission Bay, California

by

Erik Edwin Tang

Master of Science in Engineering Science (Mechanical Engineering)

University of California, San Diego, 2010

Professor Sarah Gille, Chair

Determining trajectories of mussel larvae by in situ methods has been a long standing and difficult problem in biological oceanography because of small larval size and high larval dilution rates. To better understand particle trajectories, a hydrodynamic circulation model, ADvanced CIRCulation (ADCIRC), is used to solve the vertically integrated shallow-water equations. A fourth-order Runge-Kutta method is combined with ADCIRC velocity output to advect particles, simulating advection of mussel larvae that originate in Mission Bay, California. Ensemble averages in particle termination locations are then taken to determine changes in trajectories in response to changes in surface stress, bottom stress, release time, and release location. Release from two separate parts of the bay, Dana Landing and Marine Sanctuary, are studied.

It is found that surface stress, in the form of either a varying wind or a westward wind, advects particles toward the mouth of the bay. However, a varying wind release does not affect particles from Marine Sanctuary as much as those from Dana Landing. Increasing bottom stress is found to hinder particle advection toward the mouth of the bay for particles originating at Dana Landing or Marine Sanctuary. Particle trajectories originating from Marine Sanctuary are sensitive to release times in contrast with Dana Landing trajectories. Lastly, where particles are released in Dana Landing has no major influence on trajectories.

Introduction

In marine ecosystems planktonic larvae are often responsible for the exchange of genetic material between different adult populations (Grahame and Branch 1985). Such genetic exchanges are termed "population connectivity", referring to the ability of subpopulations within spatially separated populations of the same species to exchange individuals and seed themselves (Cowen and Sponaugle 2009). Population connectivity influences population dynamics and structure, genetic diversity, and the ability of populations to withstand human exploitation (Cowen et al. 2007). Since human exploits such as overfishing, eutrophication, and habitat destruction on marine ecosystems are a growing area of concern for biodiversity conservation, understanding population connectivity is crucial for conservation.

Mussels are an ideal candidate to be studied for larval dispersal and thus population connectivity. They are common all along the California coast in large enough numbers to be empirically counted and chemically analyzed. Trace elemental analysis of the shells laid down by mussels as larvae helps to determine natal origins of the mussels. Once maturity is reached, mussels become stationary, and specimens collected from fixed sites represent mussels that have been there for their entire adult lives. This assures that data are not from a transient source.

This study focuses on mytilid mussels which live in dense beds and reside in the mid-intertidal zone along rocky shore coasts. Mussel young are dispersed as larvae and are not limited to genetic exchange between groups of the same population. In other words, populations may not be self-seeding. In fact populations may exchange

genetic material over distances of tens to thousands of kilometers (Newman and McConnaughey 1987). Two species of particular interest are the once invasive Mytilus Galloprovincialis and the currently invasive Musculista Senhousia. M. Galloprovincialis resides near the mouth of Mission Bay, California and is one of the most predominant mussels in the area. It originated from the Mediterranean and Northern Europe and resides in protected Southern California habitats and along the open coast. Estimates of M. galloprovincialis density show the densest beds reaching up to 24,000 individuals per square meter (Cáceres-Martínez and Figueras 1997**)**. Ecologically, M. galloprovincialis is a competitor for space and a large source of prey, making it an important structural component in the rocky intertidal ecosystem (Suchanek 1979). The average surface time for M. Galloprovincialis larvae is 21 days. After this period they return toward the bottom of the water column. Musculista Senhousia is found in the rear of Mission Bay with decreasing densities toward the mouth (Dexter and Crooks 2000). Musculista was first found in a salt marsh creek in the mid-1960's (MacDonald 1969) and is now prominent in intertidal and subtidal soft sediment. Musculista populations have been shown to achieve densities of 10,000 individuals per square meter (Crooks 2002). The average surface time for Musculista Senhousia is 12 days.

Both mussels have been studied in the approximately 4,200 acre Mission Bay in San Diego, California. Mission Bay was originally an estuary of the San Diego River with tidal salt marshes and numerous mud flats. This major feature of the San Diego coastline has undergone many modifications over the past 150 years by means of river diversion, dredging, and filling (Dexter and Crooks 2000). It was turned into a

recreational and commercial resource by the City of San Diego and is now the largest aquatic park on the west coast. These major physical modifications to the bay have created distinct circulation patterns throughout the bay. Bay circulation is characterized by a gradient with regions near the mouth being highly influenced by tidal flow through the inlet and areas near the back of the bay showing minimal tidal influence (Largier et al. 1997). During periods of little rainfall, insignificant volumes of freshwater reach the bay, and very long retention times are seen in the rear of the bay (Levin 1983). These circulation patterns directly influence population connectivity for the mussels that reside in Mission Bay.

In situ methods of study are constrained by practicalities of cost and scale. Computer models provide a flexible, alternative platform for experimentation (Rasmussen et al. 2009). Spatial scales of dispersal range from hundreds to thousands of kilometers for shallow-water species. Temporal scales are biologically specific to organisms being studied; that is, specific life cycles and ecological patterns of the organisms determine temporal scales. These temporal scales require studies to be conducted such that proper surface times for mussels are considered as well as long enough times for population connectivity to be understood. Time scales that influence populations on genetic scales and ecologic scales can differ and therefore must be considered for marine conservation (Cowen et al. 2007**)**. Because these scales are not always practical for physical application and because of the current lack of spatial larval information, model simulations are a valuable tool. These simulations should be made with varying physical parameters and varying time scales to determine which scales are appropriate for tracking passive particle movement and which scales lead to

subpopulation interaction. A multidisciplinary approach should be adopted to fully understand natal origins. Combinations of trace elemental fingerprinting, demographic approaches and numerical simulations will provide the greatest breadth of understanding of population connectivity. Ultimately, hydrodynamic modeling allows for the prediction of passive larval transport and the influence of specific sources of variation against which empirical results obtained through trace elemental fingerprinting and realized connectivities can be checked.

From fall 1979 to spring 1980, drift tubes were released in Mission Bay to determine larval surface water transport and dispersal potential. Drifters traveled hundreds of kilometers north and south of their starting locations in the bay suggesting the potential for population connectivity (Levin 1983). Motivated by these findings, the present study aims to create a model that simulates passive particle transport of Mytilus Galloprovincialis and Musculista Senhousia in the vicinity of Mission Bay, California. Bay-ocean particle transport has been shown to be influenced by tidal phase, wind magnitude, wind direction, and particle placement relative to the bay (Luettich et al. 1999). A sensitivity analysis in response to bottom stress showed variations in water surface elevation and velocity fields (Dill 2007). To understand the effects of these forcings on particle trajectories, a 2-D finite element code, ADvanced CIRCulation (ADCIRC), is used to provide depth-averaged velocities to a particle tracking code simulating advection. The hypothesis behind this work is that mussel larvae can leave Mission Bay, the bay circulation is forced by wind, and that wind forcing is more important than bottom stress, particle origin, or tidal release time in determining particle trajectories. Specifically, this study seeks i) to obtain stable

simulations in ADCIRC for the Mission Bay grid, ii) to provide insight on particle trajectories influenced by surface and bottom stresses, iii) to explore the effect of temporal and spatial variations on trajectories, and iv) to model realistic conditions needed to advect particles out of the bay.

Methodology

I. ADCIRC

A two-dimensional, depth-integrated, barotropic, time-dependent, long wave, hydrodynamic circulation model, ADCIRC, is used to solve the vertically integrated shallow water equations. ADCIRC is able to accurately represent domains such as deep oceans, continental shelves, coastal seas, estuarine systems, and other water bodies with complicated boundaries. Typical ADCIRC applications include modeling tides and wind-driven circulation (Luettich et al. 1999), analysis of hurricane storm surge and flooding (Ebersole et al. 2009), dredging feasibility and material disposal studies (Hench et al. 1995), larval transport studies (Luettich et al. 1998) and near shore marine operations (Weidemann et al. 2004).

The four, non-linear, coupled partial differential equations solved by ADCIRC originate from the Navier-Stokes equations for conservation of mass and momentum for an incompressible fluid.

$$\frac{\partial u}{\partial x}+\frac{\partial v}{\partial y}+\frac{\partial w}{\partial z}=0\ , \tag{1}$$

$$\frac{\partial u}{\partial t}+u\frac{\partial u}{\partial x}+v\frac{\partial u}{\partial y}+w\frac{\partial u}{\partial z}-fv=-\frac{\partial}{\partial x}\left[\frac{P}{\rho_o}-\mathrm{X}\right]+\frac{1}{\rho_o}\left[\frac{\partial \tau_{xx}}{\partial x}+\frac{\partial \tau_{yx}}{\partial y}+\frac{\partial \tau_{zx}}{\partial z}\right], \tag{2}$$

$$\frac{\partial v}{\partial t}+u\frac{\partial v}{\partial x}+v\frac{\partial v}{\partial y}+w\frac{\partial v}{\partial z}-fu=-\frac{\partial}{\partial y}\left[\frac{P}{\rho_o}-\mathrm{X}\right]+\frac{1}{\rho_o}\left[\frac{\partial \tau_{xy}}{\partial x}+\frac{\partial \tau_{yy}}{\partial y}+\frac{\partial \tau_{zy}}{\partial z}\right], \tag{3}$$

$$\frac{\partial P}{\partial z}=-\rho g\ , \tag{4}$$

where x, y are the horizontal coordinate directions, z is the vertical coordinate direction, $u(x,y,z,t)$, $v(x,y,z,t)$, $w(x,y,z,t)$ are the time-averaged velocities in the

x, y, and z directions, f is the Coriolis parameter, g is gravity, X is tidal generating potential, $P(x,y,z,t)$ is time-averaged pressure, $\rho(x,y,z,t)$ is density of water, ρ_o is reference density of water, and t is time. Eqs. 1-3 employ the Boussinesq approximation, which states that density differences are sufficiently small to be neglected, except where they appear in terms multiplied by gravity. Flows in which the horizontal scale is much greater than the vertical scale (shallow-water assumption) allow vertical accelerations to be neglected. Likewise, the effects of vertical shear of the horizontal velocity are assumed negligible, allowing the hydrostatic pressure approximation to be used. This reduces the vertical momentum equation to a relationship between the pressure and the depth (eq 4). In eqs. 1-4 the instantaneous velocities in the Navier-Stokes equations are split into average and fluctuating components. An ensemble average is taken and velocities are expressed in terms of time-averaged velocities. This method is known as Reynolds averaging. The combined viscous and turbulent Reynolds stresses are

$$\tau_{xx}(x,y,z,t) = \nu\frac{\partial u}{\partial x} - \frac{1}{\mathrm{T}}\int_0^{\mathrm{T}} u'u'\,dt\,, \tag{5}$$

$$\tau_{yx}(x,y,z,t) = \nu\frac{\partial v}{\partial x} - \frac{1}{\mathrm{T}}\int_0^{\mathrm{T}} u'v'\,dt\,, \tag{6}$$

$$\tau_{zx}(x,y,z,t) = \nu\frac{\partial w}{\partial x} - \frac{1}{\mathrm{T}}\int_0^{\mathrm{T}} u'w'\,dt\,, \tag{7}$$

$$\tau_{xy}(x,y,z,t) = \nu\frac{\partial u}{\partial y} - \frac{1}{\mathrm{T}}\int_0^{\mathrm{T}} v'u'\,dt\,, \tag{8}$$

$$\tau_{yy}(x,y,z,t) = \nu\frac{\partial v}{\partial y} - \frac{1}{\mathrm{T}}\int_0^{\mathrm{T}} v'v'\,dt\,, \tag{9}$$

$$\tau_{zy}(x,y,z,t) = \nu \frac{\partial w}{\partial y} - \frac{1}{\mathrm{T}} \int_0^{\mathrm{T}} v'w'dt\,. \tag{10}$$

Here ν is molecular viscosity, T is the integration time scale for separating turbulent and time-averaged quantities, and $u'(x,y,z,t)$, $v'(x,y,z,t)$, $w'(x,y,z,t)$ are the departures of the instantaneous turbulent velocities from the time-averaged velocities (Luettich et al. 1991).

Eq. 4 is substituted into the horizontal momentum equations (eqs. 2-3). The two resulting momentum equations and the original continuity equation are integrated over the vertical with the following boundary conditions, which originate from the definition of the substantial derivative of the vertical coordinate, z:

$$w = \frac{\partial \zeta}{\partial t} + u\frac{\partial \zeta}{\partial x} + v\frac{\partial \zeta}{\partial y} \qquad \text{(at the free surface)}, \tag{11}$$

$$w = -\left[\frac{\partial h}{\partial t} + u\frac{\partial h}{\partial x} + v\frac{\partial h}{\partial y}\right] \quad \text{(at the ocean floor)}, \tag{12}$$

producing

$$\frac{\partial H}{\partial t} + \frac{\partial (UH)}{\partial x} + \frac{\partial (VH)}{\partial y} = 0\,, \tag{13}$$

$$\frac{\partial U}{\partial t} + U\frac{\partial U}{\partial x} + V\frac{\partial U}{\partial y} - fV = -g\frac{\partial[\zeta + P_s/g\rho_o - \alpha\eta]}{\partial x} + \frac{\tau_{sx}}{H\rho_o} - \frac{\tau_{bx}}{H\rho_o} + \frac{M_x}{H} - \frac{D_x}{H} - \frac{B_x}{H}\,, \tag{14}$$

$$\frac{\partial V}{\partial t} + U\frac{\partial V}{\partial x} + V\frac{\partial V}{\partial y} - fU = -g\frac{\partial[\zeta + P_s/g\rho_o - \alpha\eta]}{\partial y} + \frac{\tau_{sy}}{H\rho_o} - \frac{\tau_{by}}{H\rho_o} + \frac{M_y}{H} - \frac{D_y}{H} - \frac{B_y}{H}\,. \tag{15}$$

Here $U \equiv \frac{1}{H}\int_{-h}^{\zeta} u dz$ and $V \equiv \frac{1}{H}\int_{-h}^{\zeta} v dz$ represent depth-averaged velocities in the x and y directions, $H = \zeta + h$ is total water column thickness, h is bathymetric depth

(distance from the geoid to the bottom), α is the effective Earth elasticity factor, η is Newtonian equilibrium potential and ζ is free surface departure from the geoid. Momentum dispersion is defined by

$$D_x \equiv \frac{\partial D_{uu}}{\partial x} + \frac{\partial D_{uv}}{\partial y}, \tag{16}$$

and

$$D_y \equiv \frac{\partial D_{uv}}{\partial x} + \frac{\partial D_{vv}}{\partial y}, \tag{17}$$

with

$$D_{uu} = \int_{-h}^{\zeta} (u-U)(u-U)dz, \tag{18}$$

$$D_{uv} = \int_{-h}^{\zeta} (u-U)(v-V)dz, \tag{19}$$

$$D_{vv} = \int_{-h}^{\zeta} (v-V)(v-V)dz. \tag{20}$$

Vertically-integrated lateral stress gradients are defined as

$$M_x \equiv \frac{\partial H\tau_{xx}}{\partial x} + \frac{\partial H\tau_{yx}}{\partial y}, \tag{21}$$

and

$$M_y \equiv \frac{\partial H\tau_{xy}}{\partial x} + \frac{\partial H\tau_{yy}}{\partial y}, \tag{22}$$

where $H\tau_{xx}, H\tau_{yy}$, and $H\tau_{yx} = H\tau_{xy}$ are the vertically-integrated lateral stress, τ_{sx} and τ_{sy} are imposed surface stresses, τ_{bx} and τ_{by} are bottom stresses, and P_s is

atmospheric pressure at the sea surface. Vertically-integrated baroclinic pressure gradients are defined as

$$B_x \equiv \int_{-h}^{\zeta} b_x dz\,, \tag{23}$$

and

$$B_y \equiv \int_{-h}^{\zeta} b_y dz\,. \tag{24}$$

Following Luettich et al. (2004), baroclinic pressure gradients are defined as

$$b_x \equiv g \frac{\partial}{\partial x} \int_{z}^{\zeta} \frac{(\rho - \rho_o)}{\rho_o} dz\,, \tag{25}$$

and

$$b_y \equiv g \frac{\partial}{\partial y} \int_{z}^{\zeta} \frac{(\rho - \rho_o)}{\rho_o} dz\,. \tag{26}$$

The combination of the depth-averaged continuity (eq. 13) and momentum (eqs. 14-15) equations are known as the primitive form of the shallow water equations (PSWE) (Conner and Brebia 1976). Finite element methods are well-suited for integrating the PSWE in shallow-water domains.

Finite element solutions of the PSWE can produce artificial, short wavelength spatial oscillations leading to numerical difficulties (Gray and Lynch 1979). A wave equation model was developed to suppress errors due to short wavelength spatial noise without use of artificial means (Lynch and Gray 1979). The oscillations were suppressed in a physically meaningful way, but the explicit time stepping approach used to solve the wave equation limited the time step because of stability constraints

rather than accuracy constraints. This led to costly simulations for highly resolved grids (Kinnmark 1986). Limitations on the time step due to stability can be strongly reduced by implementing implicit time stepping. Although the stability constraint on time step is reduced, computational effort per time step is generally increased because the matrix equations created require the simultaneous solution of elevation and both horizontal velocities. Additionally, the matrix equations must be re-assembled and re-solved at each time step (Kinnmark 1986). In order to remedy these issues and reduce the computational effort, a generalized wave continuity equation (GWCE) is introduced. The GWCE "decouples the solution for elevation and velocity and allows for the use of time independent matrices for the elevation solution and diagonal matrices for the velocity solution" (Luettich et al. 1991, Kinnmark 1986).

The GWCE is obtained by taking the time derivative of the primitive continuity equation (eq. 13) and adding the result to the product of eq. 13 and a weighting factor, τ_o. Applying the chain rule and rearranging terms gives

$$\frac{\partial^2 \zeta}{\partial t^2} + \tau_o \frac{\partial \zeta}{\partial t} + \frac{\partial \tilde{J}_x}{\partial x} + \frac{\partial \tilde{J}_y}{\partial y} - UH \frac{\partial \tau_o}{\partial x} - VH \frac{\partial \tau_o}{\partial y} = 0, \tag{27}$$

$$\tilde{J}_x = H \frac{\partial U}{\partial t} + U \frac{\partial \zeta}{\partial t} + \tau_o UH, \tag{28}$$

$$\tilde{J}_y = H \frac{\partial V}{\partial t} + V \frac{\partial \zeta}{\partial t} + \tau_o VH. \tag{29}$$

The vertically-integrated momentum equations (eqs. 14-15) are substituted into eq. 28 and eq. 29 resulting in

$$\tilde{J}_x = J_x - gh \frac{\partial \zeta}{\partial x}, \tag{30}$$

$$\tilde{J}_y = J_y - gh\frac{\partial \zeta}{\partial y}, \tag{31}$$

$$\begin{aligned} J_x = &-Q_x\frac{\partial U}{\partial x} - Q_y\frac{\partial U}{\partial y} + fQ_y - \frac{g}{2}\frac{\partial \zeta^2}{\partial x} - gH\frac{\partial [P_s/g\rho_o - \alpha\eta]}{\partial x} + \frac{\tau_{sx}}{\rho_o} - \frac{\tau_{bx}}{\rho_o} \\ &+ M_x - D_x - B_x + U\frac{\partial \zeta}{\partial t} + \tau_o Q_x \end{aligned}, \tag{32}$$

$$\begin{aligned} J_y = &-Q_x\frac{\partial V}{\partial x} - Q_y\frac{\partial V}{\partial y} + fQ_x - \frac{g}{2}\frac{\partial \zeta^2}{\partial y} - gH\frac{\partial [P_s/g\rho_o - \alpha\eta]}{\partial y} + \frac{\tau_{sy}}{\rho_o} - \frac{\tau_{by}}{\rho_o} \\ &+ M_y - D_y - B_y + V\frac{\partial \zeta}{\partial t} + \tau_o Q_y \end{aligned}, \tag{33}$$

where $Q_x, Q_y \equiv UH, VH$ are the *x*, *y* directed fluxes per unit width, respectively. Eqs. 27, 30 and 31 comprise the GWCE. The vertical profile of the horizontal velocity is required to evaluate the momentum dispersion terms (D_x, D_y). In the 2D formulation of ADCIRC, these terms are assumed negligible in the GWCE and momentum equations. Because of this, momentum dispersion terms are dropped in calculations.

The form ADCIRC solves for directly is the weighted residual form of the GWCE. Taking eq. 27, multiplying each term by a weighting function and integrating over the horizontal computational domain produces

$$\left\langle \frac{\partial \zeta^2}{\partial t^2}, \phi_j \right\rangle + \left\langle \tau_o \frac{\partial \zeta}{\partial t}, \phi_j \right\rangle + \left\langle \frac{\partial \tilde{J}_x}{\partial x}, \phi_j \right\rangle + \left\langle \frac{\partial \tilde{J}_y}{\partial y}, \phi_j \right\rangle - \left\langle UH\frac{\partial \tau_o}{\partial x}, \phi_j \right\rangle - \left\langle VH\frac{\partial \tau_o}{\partial y}, \phi_j \right\rangle = 0 \tag{34}$$

where the inner product notation, $\langle\ \rangle$, is defined as

$$\left\langle \gamma, \phi_j \right\rangle \equiv \int_\Omega \gamma \phi_j d\Omega, \tag{35}$$

where ϕ_j is a weighting function, and Ω is horizontal computational domain.

Integrating by parts the terms involving $\tilde{J}_x, \tilde{J}_y$ in eq. 34 and substituting eq. 30 and eq. 31 into the result produces the weighted residual form of the GWCE:

$$\left\langle \frac{\partial^2 \zeta}{\partial t^2}, \phi_j \right\rangle + \left\langle \tau_o \frac{\partial \zeta}{\partial t}, \phi_j \right\rangle - \left\langle gh \frac{\partial \zeta}{\partial x}, \frac{\partial \phi_j}{\partial x} \right\rangle - \left\langle gh \frac{\partial \zeta}{\partial y}, \frac{\partial \phi_j}{\partial y} \right\rangle + \left\langle J_x, \frac{\partial \phi_j}{\partial x} \right\rangle + \left\langle J_y, \frac{\partial \phi_j}{\partial y} \right\rangle + \left\langle Q_x \frac{\partial \tau_o}{\partial x}, \phi_j \right\rangle + \left\langle Q_y \frac{\partial \tau_o}{\partial y}, \phi_j \right\rangle - \int_\Gamma \left[\frac{\partial Q_N}{\partial t} + \tau_o Q_N \right] \phi_j d\Gamma = 0 \quad (36)$$

where Q_n is the outward flux per unit width normal to the boundary, and Γ is the boundary of the computational domain (Luettich et al. 2004). These continuity and momentum equations are discretized in time using the finite difference method then in space using the finite element method. Free surface elevations are obtained by solving the depth-averaged continuity equation while depth-averaged velocities are obtained from solving the vertically-integrated momentum equations.

In the derivation of the shallow water equations, the hydrostatic assumption was utilized limiting the application of these equations to flows where the vertical acceleration can be neglected. Vertically stratified fluids, super critical flows, or flows where near-field effects such as flow separation are important cannot be analyzed using the shallow-water equations (Dill 2007).

II. Track Particles

Tracking the dispersal trajectories of marine invertebrate larvae is difficult due to their small size and high dilution rates. Simulated Lagrangian particle trajectories aid in flow visualization and modeling of transport phenomena. An advective particle tracking code (Hill 2007) has been used to analyze and compare dispersal patterns of larvae in Mission Bay, California. Velocity output from ADCIRC is used to track

particles through an unstructured 2-D triangular grid using the fourth-order Runge-Kutta method (RK4), an explicit method of weighted slopes with the greatest influence by slopes at the midpoint. In the advective scheme,

$$x_{n+1} = x_n + \frac{1}{6}(\Delta x_1 + 2\Delta x_2 + 2\Delta x_3 + \Delta x_4), \tag{37}$$

$$\Delta x_1 = \Delta t U(x_n, t_n), \tag{38}$$

$$\Delta x_2 = \Delta t U(x_n + \frac{\Delta x_1}{2}, t_n + \frac{\Delta t}{2}), \tag{39}$$

$$\Delta x_3 = \Delta t U(x_n + \frac{\Delta x_2}{2}, t_n + \frac{\Delta t}{2}), \tag{40}$$

$$\Delta x_4 = \Delta t U(x_n + \Delta x_3, t_n + \Delta t), \tag{41}$$

where t is the time, Δt is the time step between ADCIRC velocity outputs, and $U(x,t)$ is velocity. Advection in the y-direction is analogous to the x-direction.

Mission Bay

Because of the spatial variability of the finite element method, highly flexible, unstructured grids are created and handled by ADCIRC. Areas with relatively simple flow characteristics have a lower resolution, and areas with complicated characteristics have a higher resolution. Mission Bay is represented by a grid consisting of 16,496 nodes and 30,797 triangular elements with bathymetry from the San Diego Parks and Recreation Department (fig. 1).

For this study, 269 particles are placed along the coast of Dana Landing (fig. 2) and 80 particles along Marine Sanctuary (fig. 3) in Mission Bay. Following release each particle is tracked to see which region of the bay it reaches under specific forcings (tables 1-2). Four specific regions (fig. 4) are identified that particles

commonly reach: west (W), inland (I), center (C) and Dana Landing (DL). Four specific points in the tidal cycle are established for particle release. ADCIRC spins up from rest and during this period there are strong model fluctuations in velocity and elevation. This period is known as the 'ramp' period. A dynamic steady-state is desired before velocities are used in the advection scheme. Particles are therefore released after the five-day ramp, or later in the model run at the highest high tide point, at the lowest low tide point, and at the neutral tide. Release at the highest high tide uses velocities starting from the highest high tide point in the velocity time series. The highest high tide is determined at the time step that produces the largest surface elevation. Release at the lowest low tide utilizes velocities starting from the lowest surface elevation. Release at the neutral tide uses velocities when the surface elevation is closest to the free surface reference datum. All surface elevations used to determine release points in time are taken from a station set in Dana Landing. Different tidal release points allow for the examination of temporal variability in particle trajectories. All depth-averaged velocities used in calculations, regardless of release times, are taken after a five-day ramp, thus bypassing fluctuations associated with ADCIRC spinning up from zero.

Particle trajectories are analyzed for seven groups of runs originating in Dana Landing or Marine Sanctuary in Mission Bay. Each group varies in τ_o, bottom stress or both (table 1-2). Runs 1 and 2 use a linear bottom stress formulation, but run 1 has a fixed τ_o, and run 2 introduces a varying τ_o. Runs 3-7 have a varying τ_o and use a quadratic bottom stress formulation involving Manning number. For each τ_o and bottom stress scenario, 12 simulations are completed. Three wind situations are tested:

no wind, varying wind, and westward wind, and for each of these, four release times are used as described above. This makes for a total of 84 distinct run scenarios. For example one scenario uses the run 1 bottom stress with no wind and particle release during the highest high tide.

The particle advection method used does not account for larval depth changes. In areas like Beaufort Inlet, NC, during the primary migratory periods of the Atlantic menhaden (fish) the "day-night cycle and the tidal cycle have nearly the same duration" (Luettich et al. 1999). This allows larvae to move to the bottom at daybreak, avoid subsurface horizontal transport, and then move back up into the water column the following nightfall at approximately the same phase of the tide during which they left. As a result, they avoid visual predation and follow surface horizontal paths that are nearly equivalent to those of purely passive particles (Luettich et al. 1999). This vertical movement pattern is known as diurnal migration. Diurnal migration of both mussels is not known, and the impact of varying release depth is not explored. Therefore in this study only passive particle transport at the surface is considered. At the least, passive particle assumptions may represent a limiting case for larvae that can regulate their vertical position. Disregarding vertical migratory behavior is a plausible assumption when day-night and tidal cycles are similar, but the validity of this assumption has not been thoroughly tested for Mission Bay mussels.

III. Boundary Conditions and Forcings

ADCIRC can be forced with tidal potentials, meteorological conditions, freshwater inflows, and tides on the boundaries. For this study only meteorological

conditions are used to force the model. Boundary conditions utilized to solve the GWCE and momentum equations are set at the land boundaries and open boundaries.

Specified Surface Stress

Surface stress at the free surface is specified as radiation stress, atmospheric pressure forcings, or wind stress. Wind stress components are given by

$$\tau_{sx} = \tau_{wind,x} = \rho_{air} C_D U_{wind}^2 , \tag{42}$$

and

$$\tau_{sy} = \tau_{wind,y} = \rho_{air} C_D V_{wind}^2 , \tag{43}$$

where ρ_{air} is the density of air, C_D is the drag coefficient between air and the ocean surface, and U_{wind}, V_{wind} are the zonal and meridional wind velocities. When forced, the shear stress is set equal to the surface stress

$$\tau_{zx} = \tau_{sx} \tag{44}$$

and

$$\tau_{zy} = \tau_{sy} . \tag{45}$$

Wind stresses are directly input into ADCIRC from hourly wind measurements taken at the Scripps Institution of Oceanography pier in La Jolla, California from April 1, 2005 to May 31, 2005. Three wind forcings are attempted in this study: no wind, varying wind and westward wind. Density of air, ρ_{air}, is taken to be 1.3 kg m^{-3} and the drag coefficient between air and the ocean surface, C_D, is 0.0012. Varying wind represents a temporally varying and spatially constant wind field. Each node in the domain is forced with the same wind stress that varies in time (fig. 5). Varying wind

magnitude and directions are in figure 6. Westward wind imposes the largest wind that blows from east to west on each node while holding the wind field constant in time. It is both temporally and spatially uniform. A westward wind velocity of 5.26 m s^{-1} corresponding to a westward wind stress, 0.044 kg m^{-1} s^{-2}, is used. Although the westward wind forcing does not represent reality, it provides insight into whether particles can leave the bay with this extreme condition. A study by McQuaid and Phillips found that in South Africa Mytilus galloprovincialis dispersed from 12-97 km depending on the wind direction, suggesting that wind is a significant contributor in particle advection. However, 90% of settlement still occurred within 5 km of their release site (McQuaid and Phillips 2000).

Specified Bottom Stress

Traditionally a no slip condition is applied at the sea floor, but using a slip condition is numerically preferred for the equations solved by ADCIRC because it allows ADCIRC to avoid numerically resolving sharp vertical gradients of velocity components that exist near the bottom (Luettich et al. 1991). Bottom stresses are expressed as

$$\frac{\tau_{bx}}{\rho_o} = K_{slip} U \,, \tag{46}$$

and

$$\frac{\tau_{by}}{\rho_o} = K_{slip} V \,, \tag{47}$$

where k_{slip} is the slip boundary condition and can be linear or quadratic. Here k_{slip} = constant is the linear slip boundary condition and the linear drag coefficient, and

$k_{slip} = D_{slip}\sqrt{U^2 + V^2}$ is the quadratic slip boundary condition where D_{slip} is the quadratic drag coefficient. Both linear and quadratic drag coefficients are tested in model runs. For the linear case, drag coefficients were held at 0.0025. Quadratic drag coefficients were varied based on Manning number,

$$D_{slip}(t) = \frac{gn^2}{\sqrt[3]{h + \zeta(t)}}, \tag{48}$$

where n is the dimensionless Manning number, h is bathymetric depth, and $\zeta(t)$ is free surface elevation. Manning number is a roughness factor which describes the resistance of fluid to flow in natural channels and flood plains based on flow surface. It originates from the empirical Manning formula:

$$Q_{discharge} = \frac{C_u}{n} AR^{2/3} S^{1/2}, \tag{49}$$

where $Q_{discharge}$ is the flow rate, C_u is the conversion unit (1 $m^{1/3}s^{-1}$ for SI units, 1.486 $ft^{1/3}s^{-1}$ for English units), A is the channel cross-sectional area, R is the hydraulic radius, and S is the hydraulic head loss. The linear slip boundary condition is used as a lower limit on the resulting quadratic slip boundary condition due to the quadratic drag coefficient decreasing in deeper waters (Luettich et al. 2006). The constant linear and varying quadratic slip boundary conditions allows for the observation of the effects of bottom stresses on passive particle transport.

Land Boundaries

Two geographic boundaries are set on the land domain: internal and external boundary conditions. Internal boundary conditions deal with land masses or obstructions seated in the water domain such as islands. External boundary conditions

represent mainland boundaries. Both types of boundaries have strong no normal flow conditions and free tangential slip. These boundary conditions are applied by setting the normal boundary flux integral in the continuity equation and the normal velocity in the momentum equations equal to zero (Luettich et al. 2006).

Open Boundaries

Tides are a major source of energy input at the open ocean boundary nodes. The tidal cycles are formed by a combination of gravitational forces from the Earth, sun and moon and centrifugal force due to the Earth's rotation. The net effect of these forces creates the tidal cycles. In order to predict the tides, harmonic analysis is used. Harmonic analysis breaks the tide down into elementary harmonic constants, which combine into a composite tide (Hicks 2006). Five tidal constituents, M2, S2, K1, O1, and N2, are used to force the elevation on open boundary nodes. Each constituent represents a variation in the position of the Earth, moon and sun relative to each other. Open boundaries are set along rivers or oceans.

IV. Stability Considerations

Several eddy viscosities and model time steps were tested until a stable run was achieved. The working eddy viscosity is 4.6 m^2 s^{-1} with a model time step of 1 second. The factor τ_o "weights the relative contribution of the primitive and wave portions of the GWCE" (Luettich and Westerink 2006). In tests run for this study, a τ_o of 0.002 produced stable runs. This τ_o value was used as a baseline for comparison. All additional model runs utilized a bounded and spatially varying τ_o dependent on the local friction.

Results

The primary metric for this study is the particle end position (fig. 7A-B), and the analysis focuses on how changes in model parameters and forcing affect end point statistics. One approach to this analysis would have been to define a baseline case with zero wind conditions, fixed bottom stress, and a single release time, and then to examine the sensitivity of the results to changes in any one of the variables. Instead, for this study, a full range of parameter space has been explored, and rather than considering changes relative to a single baseline case, an ensemble mean approach is used. Thus, (i) in order to consider sensitivity to wind, particle counts across all bottom stresses are averaged together, (ii) to consider sensitivity to bottom stress, particle counts across all release times are averaged together, (iii) to consider sensitivity to release time, particle counts across all bottom stresses are averaged together, and finally (iv) to consider sensitivity to spatial variations in the specific release location from Dana Landing, particle counts across all release times and bottom stresses are averaged together.

Contrary to our initial expectations, none of the runs produced any particles that were able to leave the bay before being beached. Of the four designated regions where particles terminate, west is the most important, because it represents the region closest to the mouth of the bay where particles have the highest likelihood of escaping the bay. In the advection scheme utilized, there was no distinction between particles that were beached and continued to move and those that were never beached. When a particle moved onto land, velocity was obtained for that particle by interpolating

velocities from the three nearest nodes in water. Many of the particles travel over land for one of two reasons:

1. The particle positions at time t and time $t+\Delta t$ are connected by a straight line that crosses land. This does not necessarily mean that the particle travels onto land but that the temporal resolution is too coarse (fig. 8A).
2. A particle crosses onto land very close to water. It is assumed that in reality this particle would skim the land and continue to move as if it were never beached (fig. 8B).

For this analysis, beaching of particles was ignored, and termination points were taken wherever the particle trajectory ended according to the advection model. Consequently, all results are only a general estimate of particle trajectory and of patterns of motion. Suggestions on remedying particle beaching are presented in the discussion and conclusion.

General Trajectories

It is helpful to first see the common patterns in particle trajectories, without considering the effects of spatial or temporal variability or stresses. For particles released from Dana Landing with no wind forcing, 52% of particles terminate in the west region, 25% remain in Dana Landing, 20% reach the center region and 3% terminate in the inland region. Marine Sanctuary particles reside in the rear of Mission Bay where there is poor circulation. Because of this when no surface stresses are imposed, few particles are able to travel far throughout the domain. In general Marine Sanctuary particles travel to the inland or center regions of the bay.

Wind

The model is forced with varying and westward wind stress, in order to assess the impact of wind on particle trajectories. Figure 9A shows the average percent change in particles originating in Dana Landing and terminating in each section of Mission Bay when forced with a varying wind. Average percent change in particles refers to the difference in the number of particles when a wind forcing is compared to a no wind case averaged over all bottom stresses. When compared to runs with no wind, 96% of varying wind runs show an increase in west terminating particles and 68% show an increase in center terminating particles. For inland terminating particles, 46% of varying wind runs show an increase, and 54% show a decrease. Because of this, it is difficult to predict how varying wind will change inland terminating particles. A decrease in the number of particles terminating in Dana Landing is seen in 89% of varying wind runs, and the average percent change for Dana Landing terminating particles decreases with a varying wind.

Marine Sanctuary particles are also influenced by a varying wind (fig. 9B). The average number of west terminating particles varies depending on release time with 68% of all varying wind runs showing no change for west terminating particles when compared to runs with no wind. Those runs which do show a change range from a decrease of 7.5% to an increase of 10% with only one run increasing by 64%. Because of the low number of runs that produce a change and the relatively small changes in those runs, change in west terminating particles due to a varying wind is considered minor. For inland terminating particles, 43% of varying wind runs show a decrease, 36% show an increase and 21% show no change. Because these percentages

for inland terminating particles are so close, and the average percent change for inland terminating particles increase for half and decrease for half of the release times, it is difficult to determine how inland particles will change due to a varying wind. When Marine Sanctuary particles terminate in the center region, 43% of varying wind runs show an increase, 39% show a decrease, and 18% show no change. Additionally, the average percent change for center terminating particles increases indicating that center terminating particles increase with the addition of a varying wind. Regardless of wind condition, release time and bottom stress, particles released at Marine Sanctuary never terminate in Dana Landing. Due to the low number of west and Dana Landing terminating particles, center and inland regions receive the majority of particles and partially balance each other. When center particles decrease, inland particles increase and vice versa.

Results indicate that westward wind is very effective at advecting particles out of Dana Landing. The majority of runs show an increase in the number of west terminating particles and a decrease in the number of center and Dana Landing terminating particles (fig. 9C). In total, 93% of westward wind runs show an increase in west terminating particles when compared to runs with no wind. In contrast, in westward wind runs, 83% of cases show a decrease in center terminating particles and 64% show a decrease in inland terminating particles. These changes are consistent with a shift of particles away from the inland and center regions and to the west. There are no increases in Dana Landing terminating particles, and all westward wind runs show fewer than 5% of Dana Landing originating particles terminating in Dana Landing. The increase in west terminating particles for westward winds is 67% greater

than the increase for varying winds suggesting that a westward wind promotes the movement of particles toward the mouth of the bay, more so than no wind or varying wind situations.

Marine Sanctuary originating particles indicate an increase in west and center terminating trajectories for westward winds when compared to no winds (fig. 9D). Approximately 79% of all westward wind runs show an increase in west terminating particles, while 21% show no change. Center terminating particles increase for 61%, decrease for 36% and do not change for 3% of all westward wind runs. No Marine Sanctuary particles terminate in Dana Landing regardless of the wind. A westward wind affects Marine Sanctuary in the same way as Dana Landing- west and center terminating particles are increased. Inland terminating particles decrease significantly from the no wind situation because they are more likely advected toward the west. This large increase in west particles has shifted the majority of Marine Sanctuary particles from terminating in the center and inland regions to the west and center regions.

Overall when released from Dana Landing a varying wind tends to increase west and center terminating particles, decrease Dana Landing terminating particles and vary inland particles based on release time. For Marine Sanctuary particles, forcing with a varying wind results in minor changes for west and no changes for Dana Landing terminating particles. It does, however, increase center terminating particles while varying inland terminating particles based on release time. Forcing with a westward wind in both Dana Landing and Marine Sanctuary shows a large increase in west terminating particles and decreases in inland terminating particles. In Dana

Landing however, center and Dana Landing terminating particles decrease due to wind advecting the particles toward the open ocean. In Marine Sanctuary, center terminating particles increase due to westward wind advecting particles out of the rear of the bay toward the center region. Particles never terminate in Dana Landing when released from Marine Sanctuary.

Bottom Stress

Bottom stress can have a dampening effect on particle velocity and thus particle trajectory. The effects of bottom stress are explored to see how trajectory patterns may vary. Percentage of particles is the fraction of particles that originate at Dana Landing or Marine Sanctuary and terminate in a specified section of Mission Bay. For particles released in Dana Landing as bottom stress values increase, west terminating particles slightly increase until large bottom stress values are reached. At a Manning number of 0.016, west particles begin to drop off (fig. 10A). The increased bottom stress seems to greatly reduce particles abilities to advect westward toward the mouth of the bay. This drop in west terminating particles is complemented by an increase in center terminating particles (fig. 10B). As a result, particles are found mainly in the center region at the largest bottom stresses.

Influence of bottom stress on inland and Dana Landing terminating particles is minimal. In general inland terminating particles do not significantly change with increasing bottom stress. Only at the largest bottom stress, Manning number of 0.100, do inland terminating particles increase. Large bottom stress tends to keep particles in the center and inland areas of Mission Bay. Without the influence of wind, Dana Landing terminating particles are more influenced by tidal release time and are

therefore not sensitive to bottom stress in the absence of wind. When winds are considered, Dana Landing terminating particles drop to nearly zero, and the influence on bottom stress cannot be observed.

Overall the effects of bottom stress for particles released from Dana Landing become most evident at higher values for all three wind situations. West terminating particles tend to decrease as bottom stress is increased with the largest decreases corresponding to the largest bottom stress (fig. 10A). Inland terminating particles remain fairly stable as bottom stress increases but increase for high bottom stress. Center terminating particles show a fairly consistent yet minimal increase across all bottom stresses with the greatest increase at the greatest bottom stress (fig. 10B). This increase in center terminating particles is complemented by a decrease in west terminating particles. Dana Landing terminating particles show the greatest variability in relation to wind forcing, bottom stress and release time. This is because wind forcing plays a significant role in transport out of Dana Landing.

Marine Sanctuary trajectory patterns influenced by bottom stress are most evident when grouped based on wind forcing. In the absence of wind forcing for Marine Sanctuary originating particles, Dana Landing and west terminating particles are insignificant (Fig. 11A). No Marine Sanctuary particles reach these sections of the bay. Center and inland terminating particles complement each other in that when one increases the other decreases. There are no clear patterns of motion for center and inland terminating particles as bottom stress increases. It seems that particle trajectories in the absence of wind are dominated by release time more than bottom stress. It should be noted that the largest Manning number, 0.100, does lead to an

increase in inland particles and a decrease in center particles which is consistent with the effects of Manning number found for Dana Landing (fig. 11B-C).

With the addition a varying wind, west and Dana Landing terminating particles are insignificant. Center terminating particles decrease with increasing Manning number, and inland terminating particles increase (fig. 11B-C). With a westward wind, the number of west terminating particles increases dramatically, reducing the number of inland particles. Now, center and west particles complement each other and Dana Landing and inland particles are insignificant. As Manning number increases, center particles increase and west particles decrease (fig. 11A, 11C).

Overall, for Marine Sanctuary originating particles, west terminating particles decrease with increased bottom stress but only occur with a westward wind; otherwise very few west terminating particles occur. Center terminating particles tend to decrease with increasing bottom stress while inland terminating particles tend to increase. No Marine Sanctuary particles terminate in Dana Landing. Bottom stress tends to keep Marine Sanctuary particles in the inland and center region until acted on by a westward wind.

Release Time

The influence of different tidal release times on particle trajectories is explored by examining the average particle percentage in each section of Mission Bay for each release time and for each wind situation. Average particle percentage is calculated by averaging, over all bottom stresses, the percentage of particles terminating in each section of Mission Bay.

Release time for particles from Dana Landing is seen to affect the percentage of particles but not the general pattern of motion. For releases with no wind or varying wind, the west terminating particles are most likely to come from release during the neutral tide. When a westward wind is forced, release after the five-day ramp produces the greatest average of west terminating particles. Although there is some variation in the average particle percentage associated with release time for each termination location, all release times exhibit the same spatial patterns: particles are to terminate in the west, and terminations are progressively less likely as one moves to the center, inland and Dana Landing regions. This shows that in general, Dana Landing particle trajectories are minimally influenced by the chosen release times (fig. 12A-C).

There is no general pattern of motion influenced by release time in Marine Sanctuary like in Dana Landing (fig. 13A-C). Particle trajectories show much more variation for each release time with wind forcings having heavy influence. For all release times, the average percentage of particles terminating in Dana Landing is zero. The number of particles starting in Marine Sanctuary and terminating in the west are insignificant except when a westward wind is forced. In general particles from Marine Sanctuary are highly sensitive to release time and wind meaning each release time and each wind scenario will result in different termination locations. However, release during the neutral tide is seen to have particles terminate in areas of the bay which have the majority of particle terminations. Figures 13A-B have particles released during the neutral tide terminating in the inland region, and figure 13C has particles released during the neutral tide terminating in the west region. Both inland and west

regions are the dominant termination locations for their respective wind forcing. All other release times do not show this pattern for all wind scenarios.

Spatial Dependence

Release location of particles relative to a bay inlet has shown to produce differing particle trajectories in Beaufort Inlet, NC (Luettich et al. 1999). Motivated by these findings, particles are released all along Dana Landing, which is subdivided into three areas: west Dana Landing (WDL) receives 80 particles, central Dana Landing (CDL) 119 particles, and east Dana Landing (EDL) 70 particles (fig. 2). Figures 14A-C display the average percentage of particles which reach each section of Mission Bay for release from different sections of Dana Landing. Average percentage of particles is calculated by averaging the number of particles which terminate in each section of Mission Bay over all release times and bottom stresses then normalizing by the number of particles in each respective release section of Dana Landing (WDL, CDL, EDL). In the absence of wind, particles from WDL and CDL terminate, in descending order, to the west, Dana Landing, center then inland areas (fig. 14A). With a varying wind, WDL and CDL particles terminate, in descending order, to the west, center, Dana Landing and inland regions (fig. 14B). EDL originating particles with no wind (fig. 14A), a varying wind (fig. 14B) and all regions of Dana Landing originating particles with a westward wind (fig. 14C) have the same termination pattern: west, center, inland then Dana Landing areas.

Overall, particles from WDL and CDL produce similar particle trajectories while EDL particles produce similar trajectories across all wind scenarios. Regardless

of starting location, west percentages are higher than all other regions (inland, center, Dana Landing) suggesting particles prefer to move toward the west.

Discussion and Conclusion

This study considers the particle trajectories predicted for mussels in Mission Bay, California under varying surface stresses, bottom stresses, tidal release times, and spatial distributions. A two-dimensional, depth-integrated, barotropic, time-dependent, long wave, hydrodynamic circulation model, ADCIRC, is used to solve the vertically integrated shallow water equations for fluid velocity and surface elevation. Particle trajectories are computed using a fourth order Runge-Kutta method.

Particle trajectories indicate that the majority of particles originating from Dana Landing are transported to the west and center regions of Mission Bay. As wind forcings are added, the number of particles remaining in Dana Landing decreases while the numbers ending in both west and center regions increase, suggesting that varying wind and westward wind advect particles out of Mission Bay. Advection out of the bay is inhibited by bottom stress. High bottom stress corresponds to small velocities and reduced advection distances. When bottom stresses are low, particles are more likely to move toward the west region, but as bottom stress grows, the number of west trajectories decrease. This causes the number of particles terminating in the center and inland parts of the bay to increase, thus reducing the probability of particles leaving the bay.

Different release times in the tidal cycle influence the percentage of Dana Landing originating particles per region but not the overall patterns of motion; in decreasing order, particles move toward the west, center, inland and Dana Landing regions. Spatially varying where particles begin in Dana Landing show similar

trajectory patterns- particles tend toward the west and center regions.

The rear region of Mission Bay, Marine Sanctuary, does not have as much motion as areas closer to the open ocean, which are highly influenced by flows outside of the bay. These flows set up circulation patterns for areas close to the mouth but do not influence the rear of the bay. As a result, little circulation occurs. This reduces the variability in particles released from Marine Sanctuary. No Marine Sanctuary particles terminate in Dana Landing, and the majority of trajectories are concentrated in the inland and center regions. The addition of a varying wind does not significantly increase the probability that particles will reach the mouth of the bay. The minimal tidal influence of this region effectively traps particles. Wind forcing influences particle trajectories, and only under westward wind forcing are particles able to move toward the west region. In reality the likelihood of particles from Marine Sanctuary leaving the bay is very low, since constant westward wind forcing is unrealistic. Bottom stress reduces velocity in such a way as to hinder outward movement thus causing variations in whether particles will travel to the center or inland areas paralleling the effect of bottom stress in Dana Landing.

Particles that reach the west region are most likely to be advected out of Mission Bay and into the open ocean. Because the majority of particles regardless of wind forcing, bottom stress, release time, and spatial location display the tendency to move to the west, particles in Dana Landing are assumed to be able to reach the open ocean and mix with other populations. Of all varied parameters, wind forcing has the greatest influence on trajectories. According to our results, particles launched at Dana Landing can exhibit population connectivity. Marine Sanctuary particles are less likely

to show population connectivity, except under unusually strong westward wind conditions.

Because particles tend to beach, results reported here should be considered only as generalizations of possible patterns of motion. Distances between locations of a single particle for each time step can be large for cases presented in this study. It has been suggested that reducing these distances may avoid potential beaching of particles (Hill 2007). In order to achieve this, the frequency of velocity output should be reduced from every 1200 seconds to roughly every 300 seconds. This should lead to a smoothing of particle trajectories and reduce beaching. If the reduced output is not sufficient to eliminate beaching then refinement of the Mission Bay grid may be necessary. An additional alternative is to modify the advection code to account for this possible beaching. Particles that hit land should be held in their previous water location then advected once the fluid velocity is able to continue to transport the particle in water. This will provide a more realistic picture of trajectories.

Variations with depth may need to be considered using a three-dimensional version of the model, ADCIRC 3-D. ADCIRC 3-D is able to output velocity at each horizontal node for defined depth levels by solving the GWCE and 3-D momentum equations. One possibility is to examine the trajectories at different depths and compare that to the results from other methods such as elemental fingerprinting (Becker et al. 2005). For example, if elemental fingerprinting results indicate a dominant source to the south, but model trajectories show dominant southward movement at the surface and northward movement at the subsurface, that would make a case for larvae being transported subsurface. Lastly, only four tidal release times

were examined. It may be that particle trajectories show greater sensitivity to release time than seen here. Releasing particles in 20 minute increments then comparing them to the trajectories produced in this study will allow for a better understanding of the role of release time. The combination of the elimination of beaching via a smaller output time step or modification of the advection code, knowledge of trajectory variations with depth and more insight into temporal variability should produce a deeper understanding of likely mussel trajectories and connectivity.

Appendix

Table 1. Constant Run Parameters: Run parameters which remain constant for all runs. Westward wind velocity is not applied to all runs but is held constant at 5.26ms^{-1} when a westward wind is forced. Bottom friction is the linear drag coefficient when a linear bottom stress is used. Quadratic drag coefficients use Manning number.

Total Run Time (days)	45
Model Time Step (s)	1
ADCIRC Velocity Output (s)	1200
Ramp (Days)	5
Eddy Viscosity (m^2 s^{-1})	4.65
Bottom Friction	0.0025
Westward Wind Velocity (m s^{-1})	5.26

Table 2. Varying Run Parameters: Run Parameters which vary between runs. Runs 1 and 2 use a linear drag coefficient. Runs 3-7 use a quadratic drag coefficients involving Manning number.

Run No.	τ_o **Range**	**Manning Number**
1	0.002	None
2	0.005 - 0.2	None
3	0.005 - 0.2	0.007
4	0.005 - 0.2	0.013
5	0.005 - 0.2	0.016
6	0.005 - 0.2	0.050
7	0.005 - 0.2	0.100

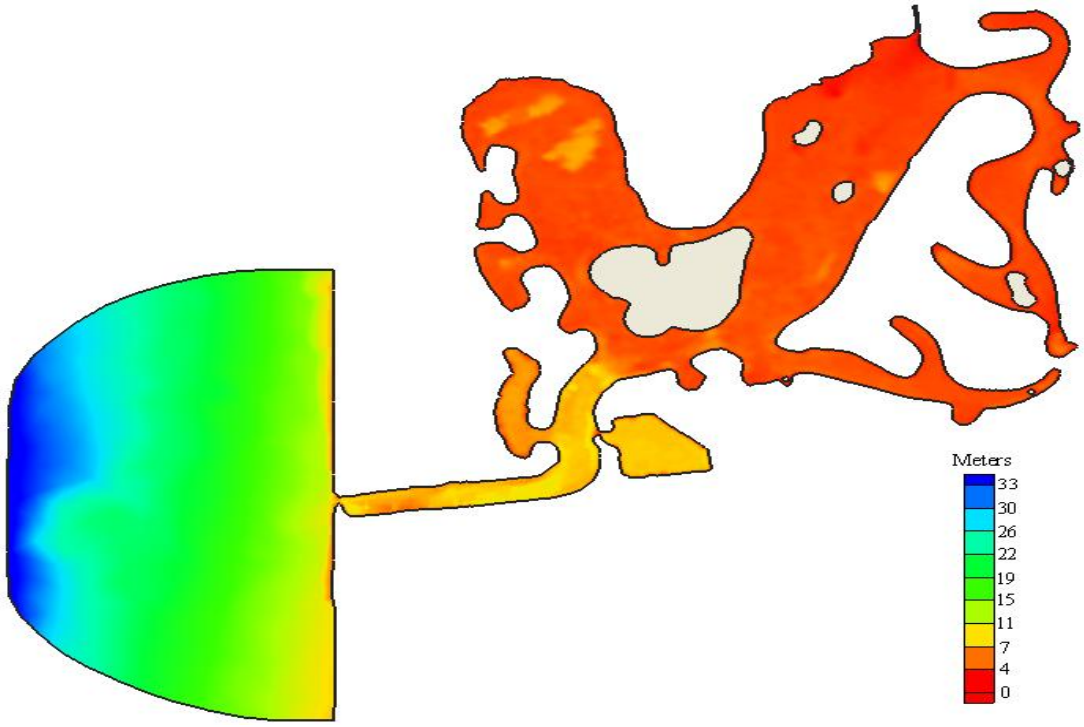

Figure 1. Mission Bay Bathymetry: Bathymetric depths with respect to the geoid. Positive values are below the geoid and negative values are above the geoid. Min: -3m, Max: 35m. In calculations the minimum water depth used is 1.5 m regardless of actual bathymetry.

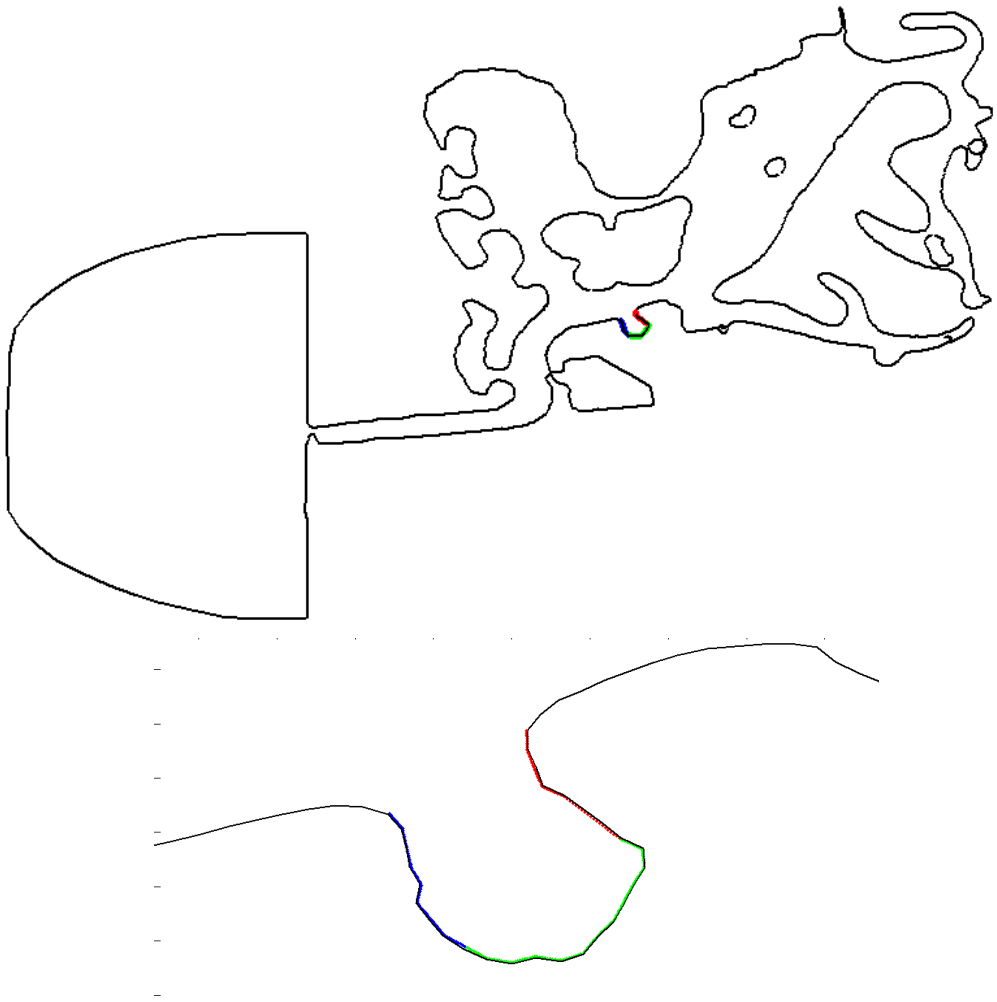

Figure 2. Dana Landing: The three divisions of Dana Landing are shown here. West Dana Landing is colored blue. Central Dana Landing is colored green. East Dana Landing is colored red. There are a total of 269 particles spread throughout Dana Landing with particles 1-80 on the west (blue), 81-169 in the center (green), and 170-269 on the east (red).

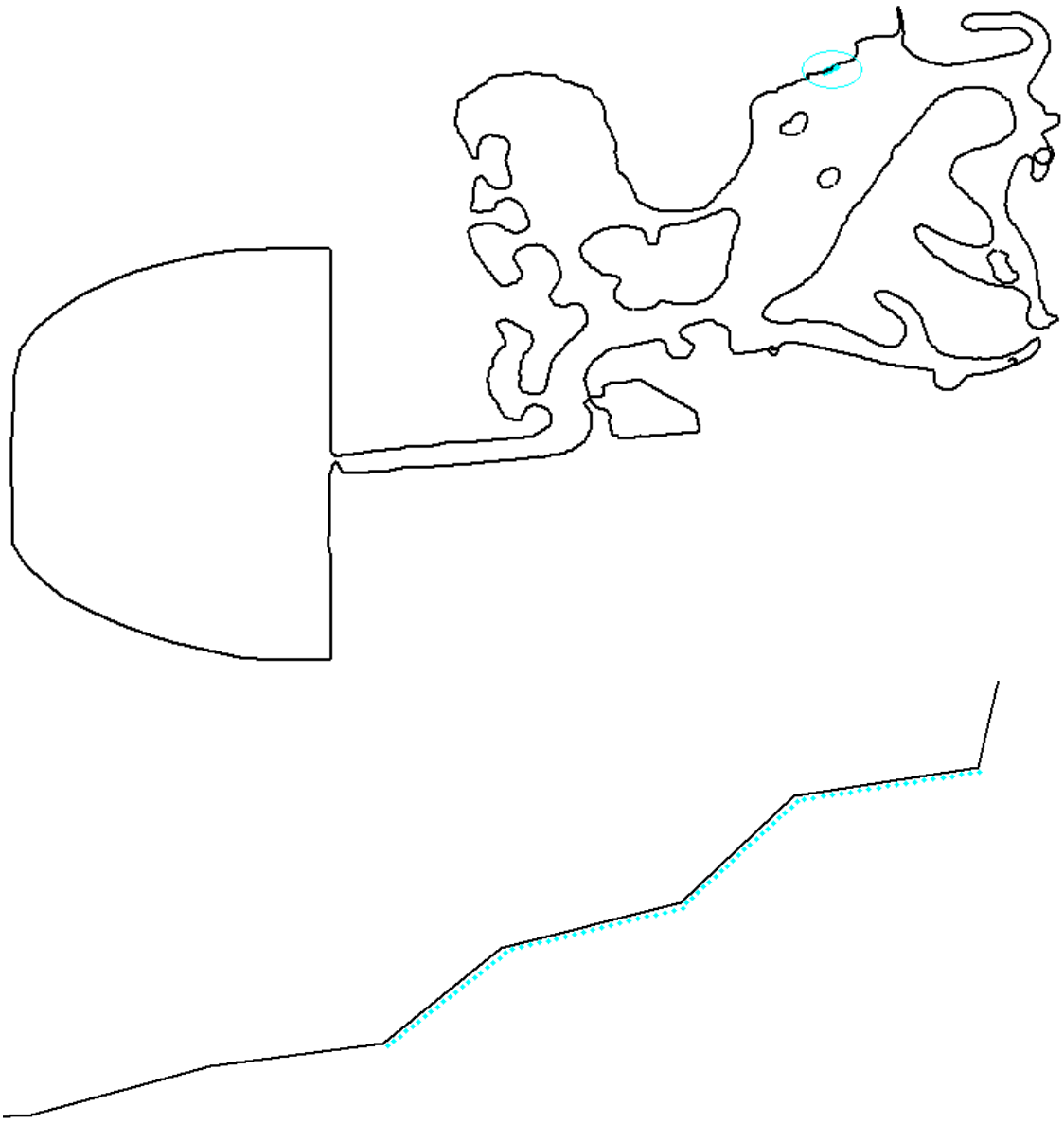

Figure 3. Marine Sanctuary: Particles (cyan) placed along Marine Sanctuary.

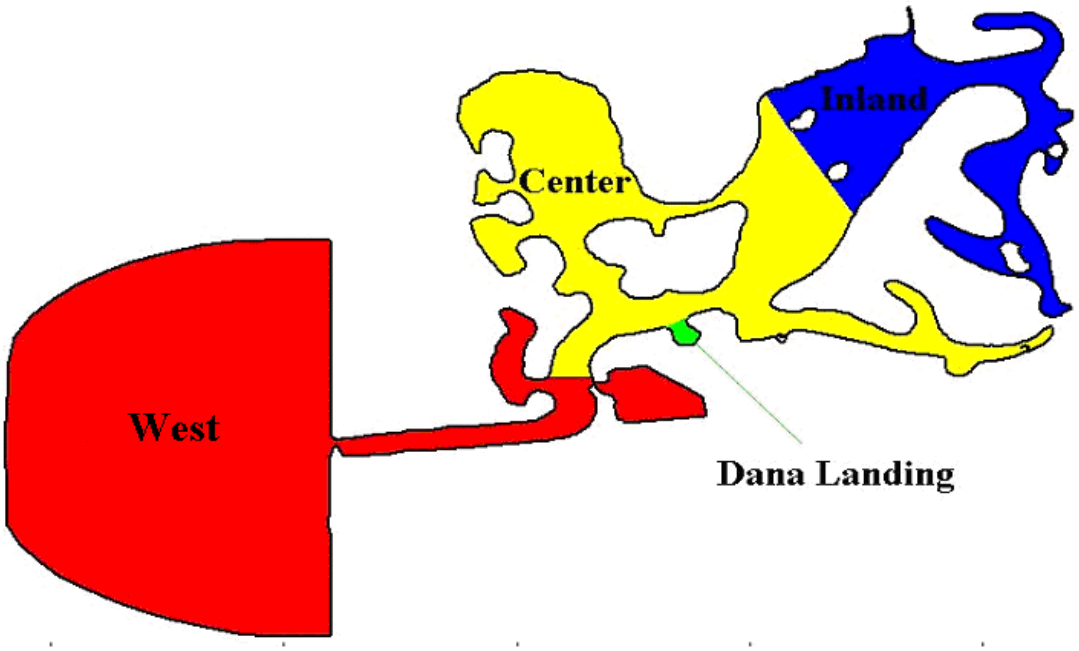

Figure 4. Mission Bay Divisions: Mission Bay is split into four distinct regions where particles terminate. West (red) is the mouth and near mouth regions of the Bay. The inland area (blue) is the upper region of the bay east of the two small islands. Center (yellow) is the region west of the two small islands on the right side of the domain and east of the bay mouth. Dana Landing (green) is the small inlet at the center of the domain.

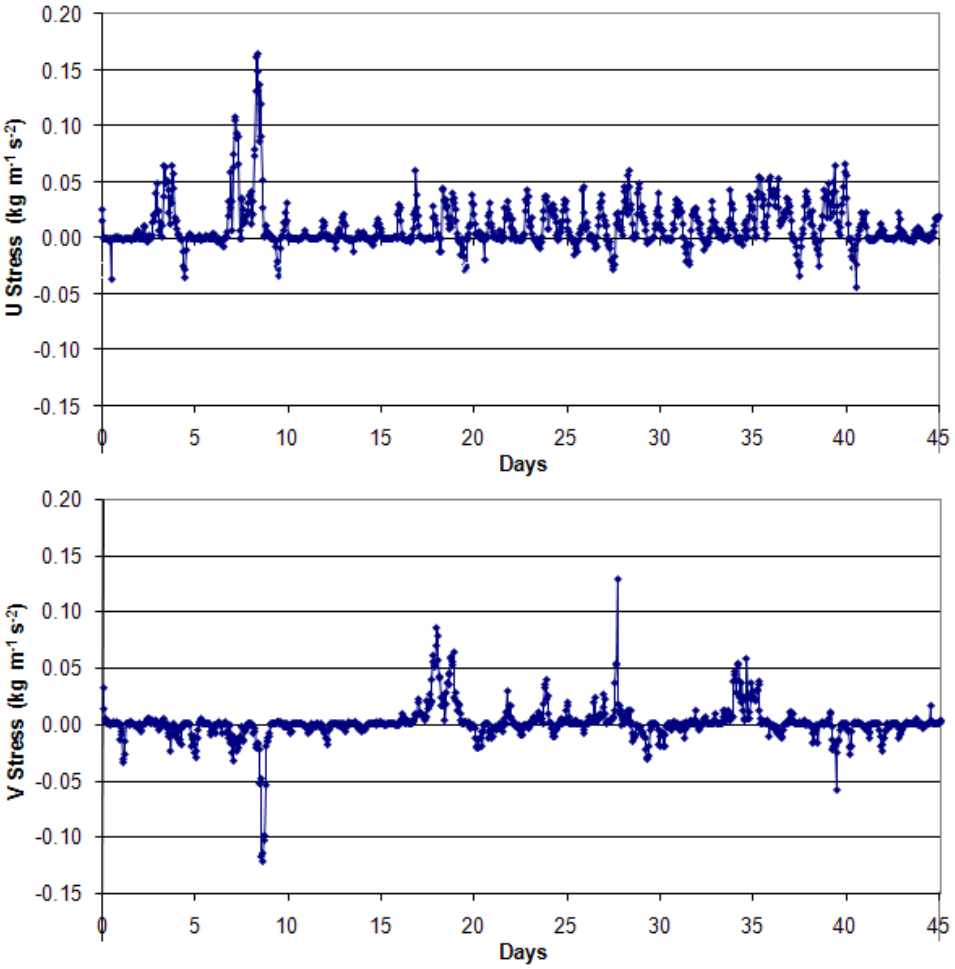

Figure 5. Wind Stress: Velocity surface stress values for 45 days. An oceanographic sign convention is used where positive values are blowing toward the east or north, and negative values are blowing toward the west or south. Max Northward Stress: 0.129 kg m^{-1} s^{-2}, Max Southward Stress: 0.121 kg m^{-1} s^{-2}, Max Westward stress: 0.044 kg m^{-1} s^{-2}, Max Eastward Stress: 0.165 kg m^{-1} s^{-2}

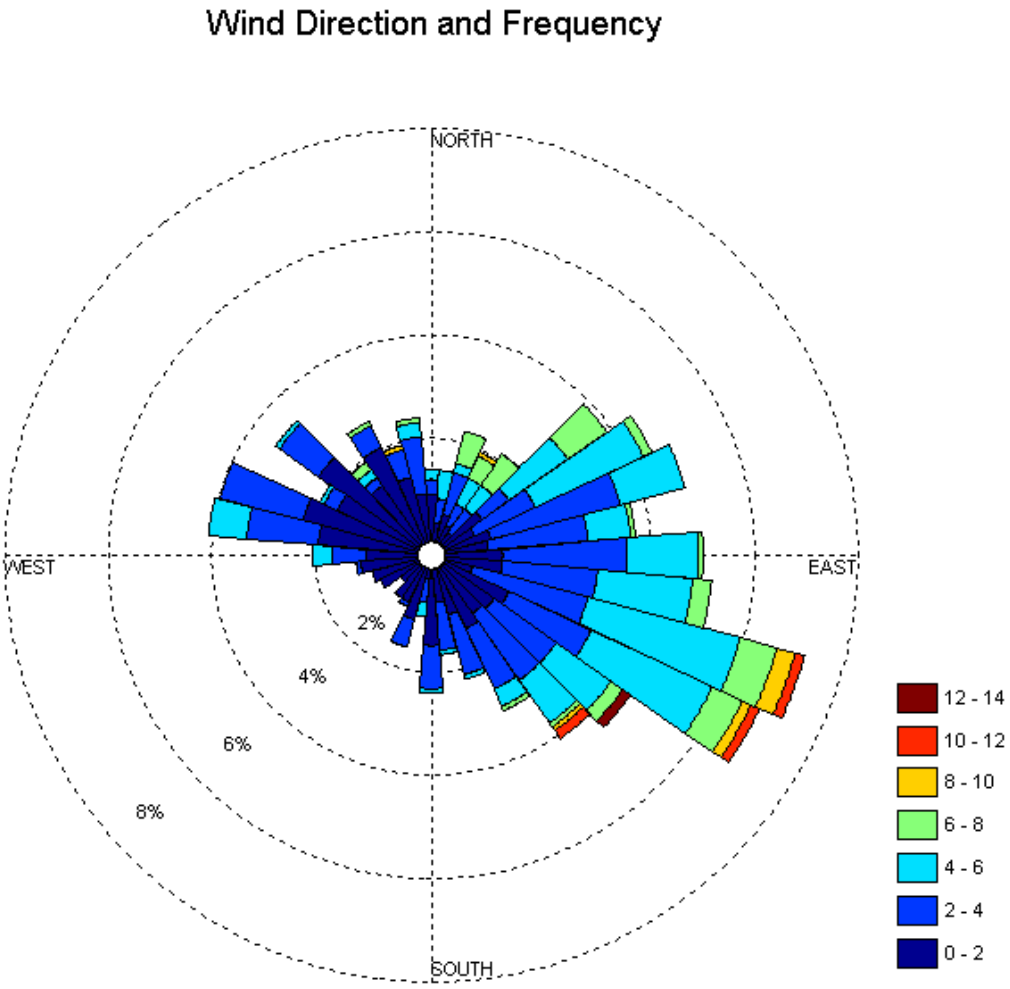

Figure 6. Wind Direction, Frequency and Magnitude Histogram: Histogram of directions varying wind blows for each hour over 45 days. Wind directions are measured using a standard oceanographic convention. 0 and 360 degrees represent a wind blowing to the east. 90 degrees represents a wind blowing to the north. 180 degrees represents a wind blowing to the west. 270 degrees represents a wind blowing to the south. All 'arms' of the diagram represent directions the winds are blowing toward. Concentric circles represent the frequency in percentages velocities occur. Colors represent wind speeds in meters per second with the area of each color representing a particular velocity range. The greater the color per arm, the greater the frequency of that velocity in a particular direction.

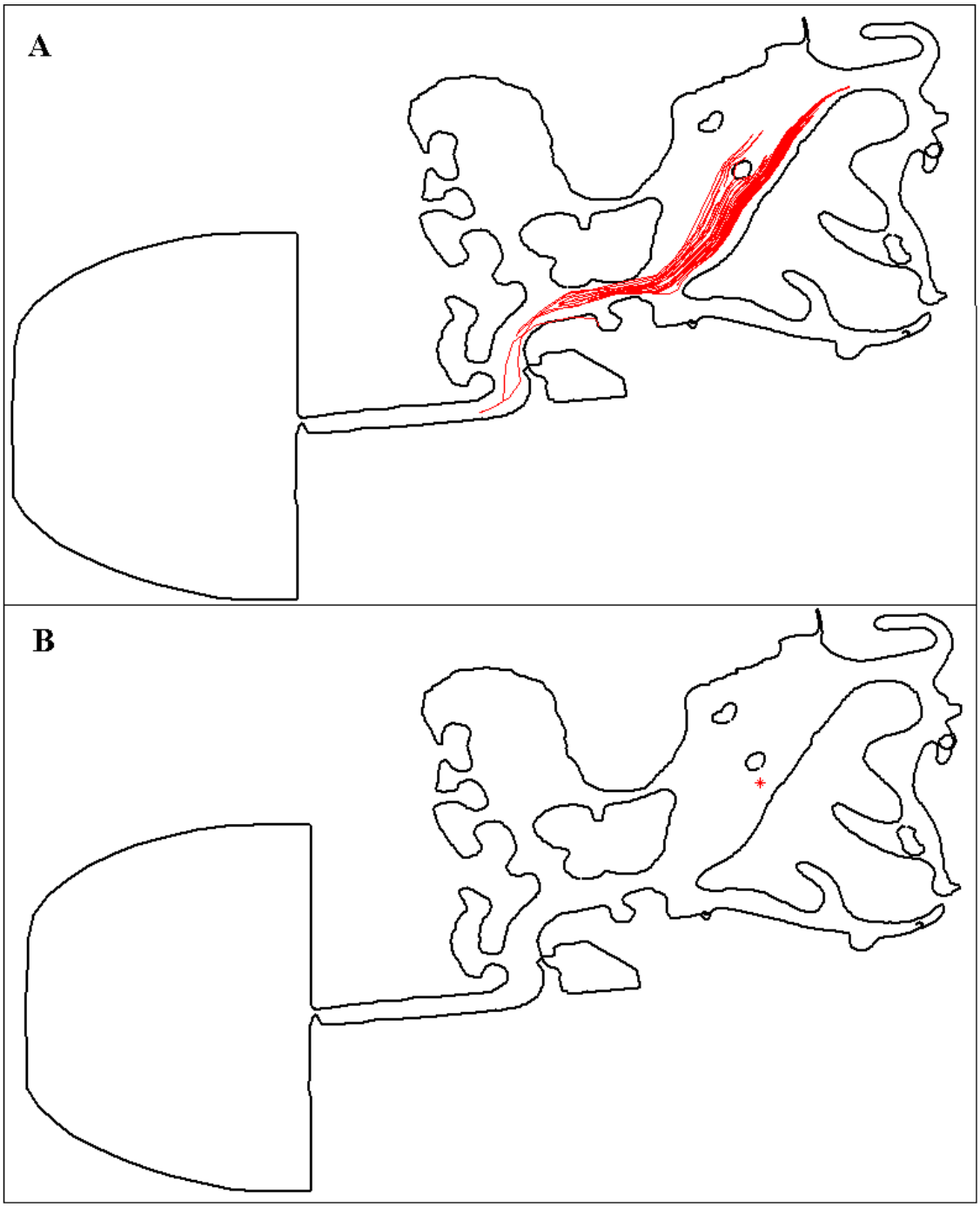

Figure 7. Particle Trajectory and End Position: A sample trajectory for a particle released from Dana Landing (A) and its termination location (B)

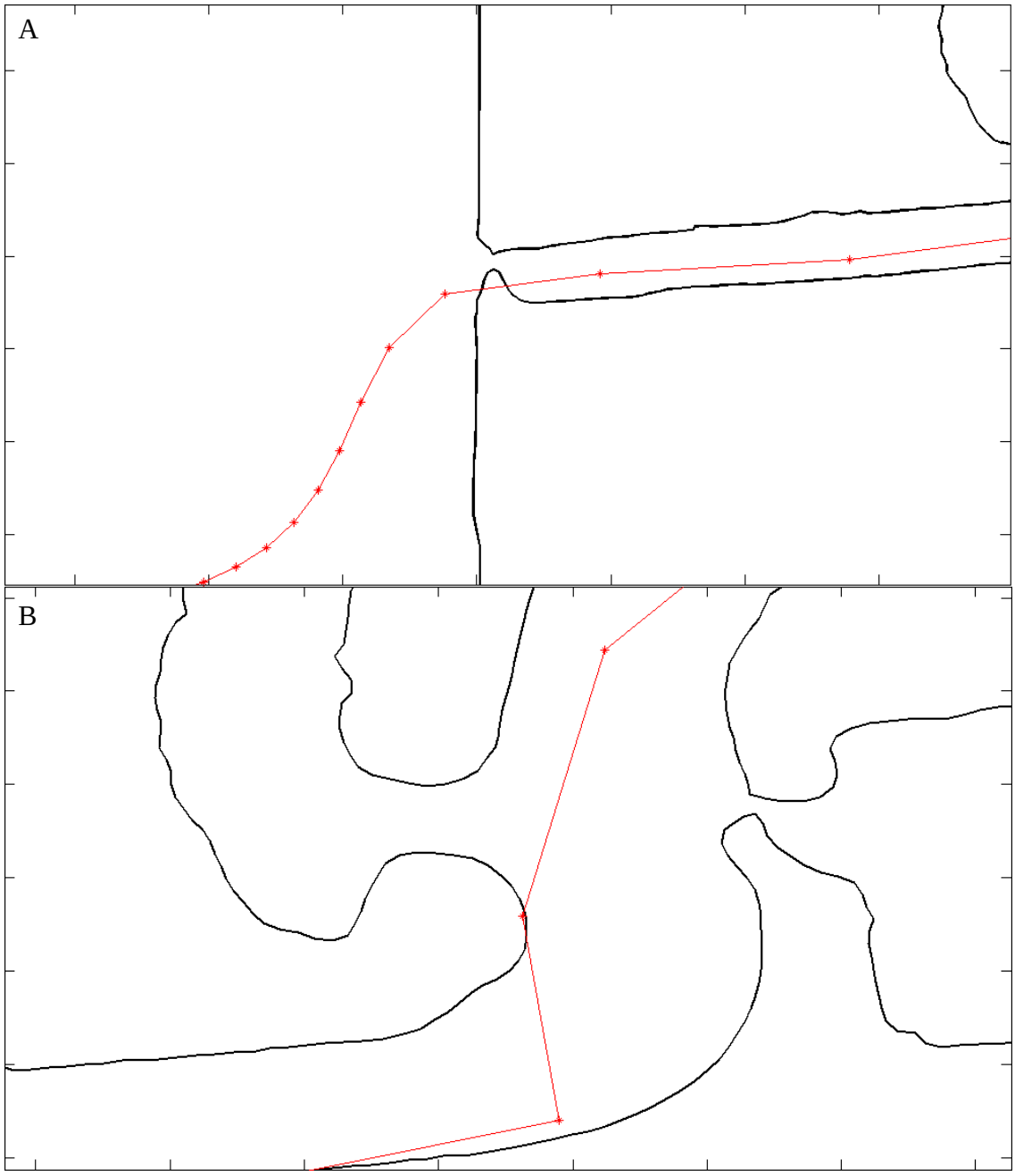

Figure 8. Particle Beaching: Beaching of particles in Mission Bay occur in two common ways. First, particles may move over land because two successive points are on opposite sides of land. When the two points are connected by a straight line it appears as if the particle has taken that path (A). Second, a particle may skim land and continue moving. The particle is actually shown to be on land but in reality the particle will most likely be in water (B).

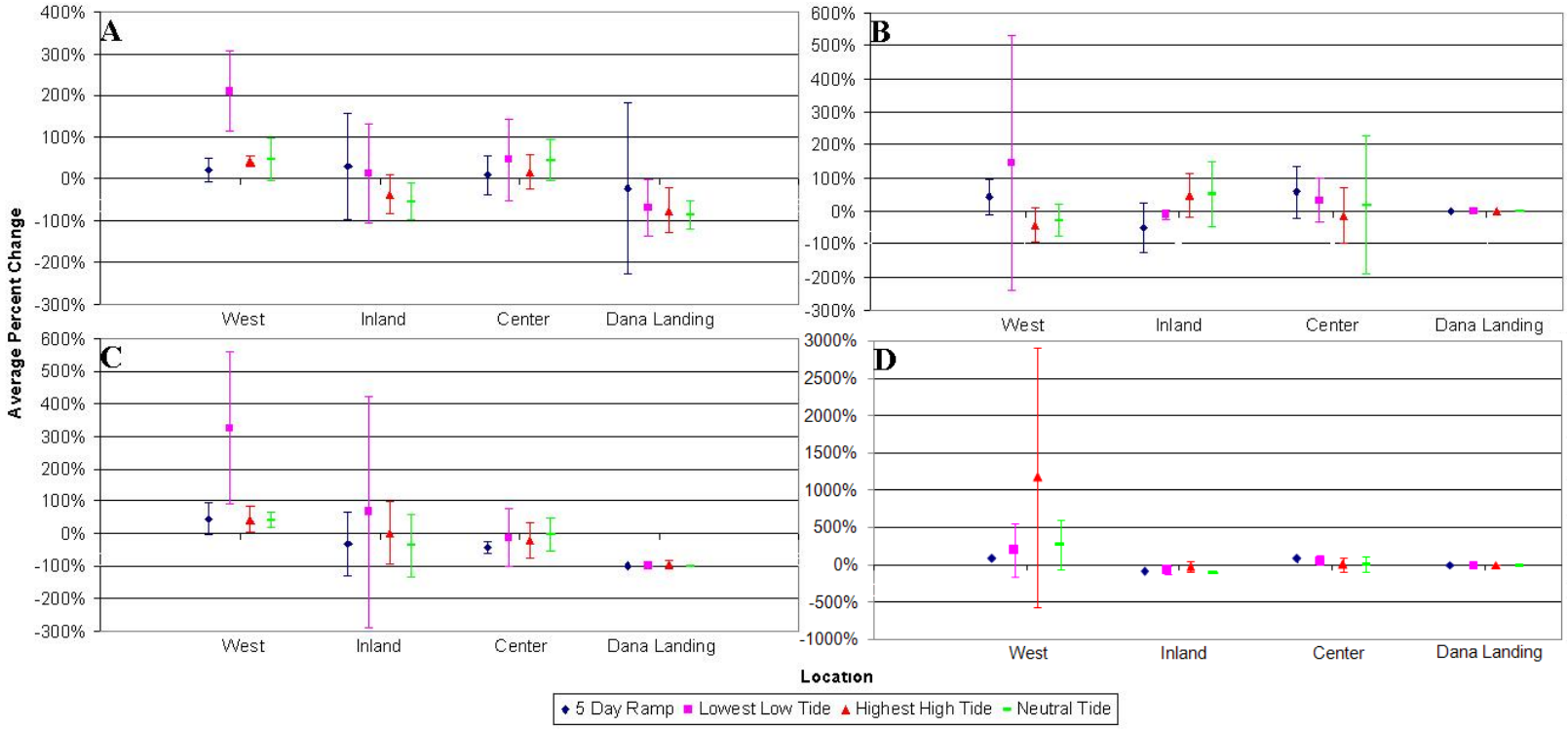

Figure 9. Effect of Adding Wind on Particle Trajectories: The average percent change in the number of particles terminating in each section of Mission Bay due to the addition of a varying or westward wind is shown for each release time. Average percent change is calculated by comparing the number of terminating particles with and without wind for each section of the bay. For Particles starting in Dana Landing, (A) no wind vs. varying wind and (C) no wind vs. westward wind are shown. For Particles starting in Marine Sanctuary, (B) no wind vs. varying wind and (D) no wind vs. westward wind are shown. Marker points represent average values and error bars are one standard deviation above and below values. Positive values represent an increase in particles due to wind. Negative values represent a decrease in particles due to wind.

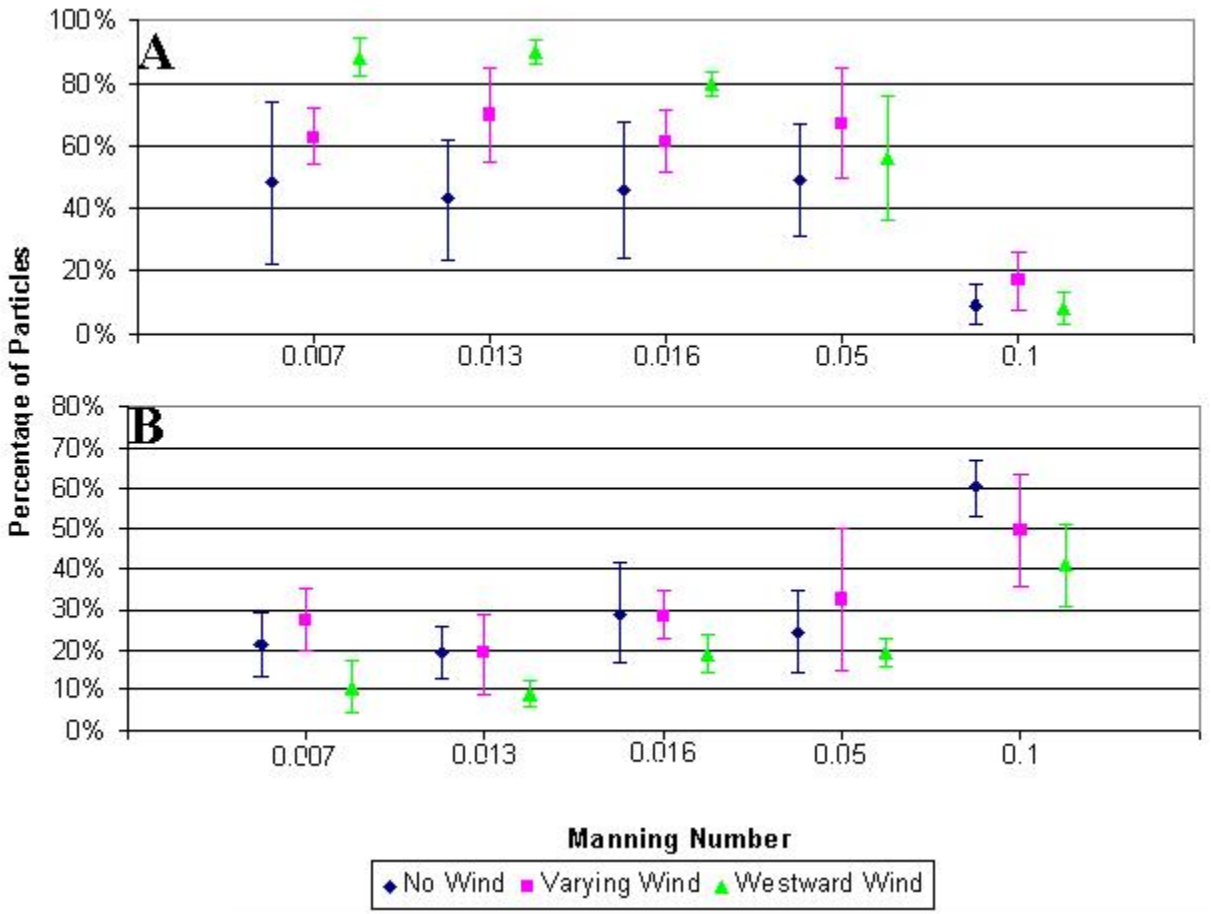

Figure 10. Effect of Increasing Bottom Stress on West and Center Trajectories from Dana Landing: The percentage of particles averaged over all release times from Dana Landing which flow to the west (A) and center (B) regions as bottom stress is increased is shown for each wind scenario. Error bars are one standard deviation above and below values.

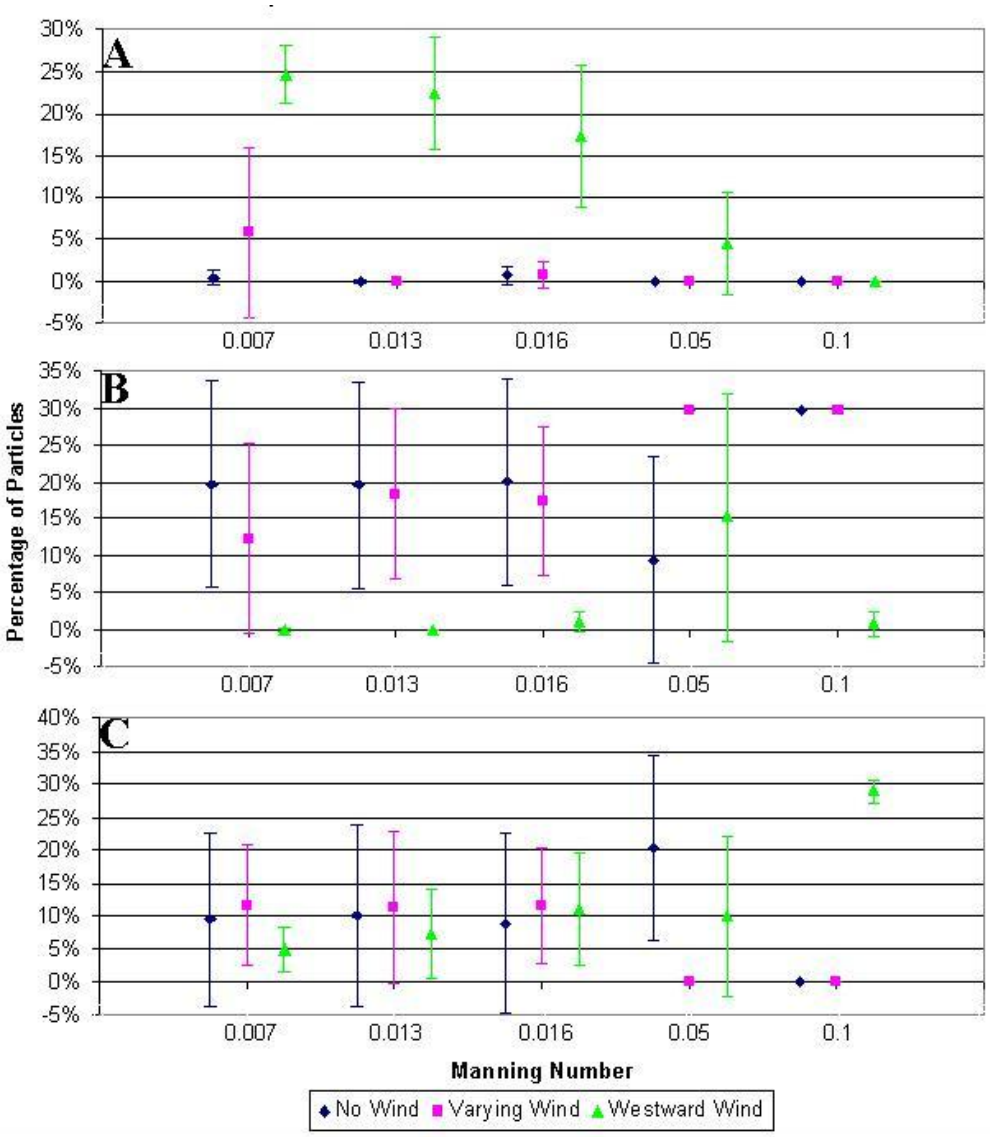

Figure 11. Effect of Increasing Bottom Stress on Marine Sanctuary Particles: The percentage of particles averaged over all release times from Marine Sanctuary which flow to the west (A), inland (B) and center (C) regions as bottom stress is increased is shown for each wind scenario. Error bars are one standard deviation above and below values.

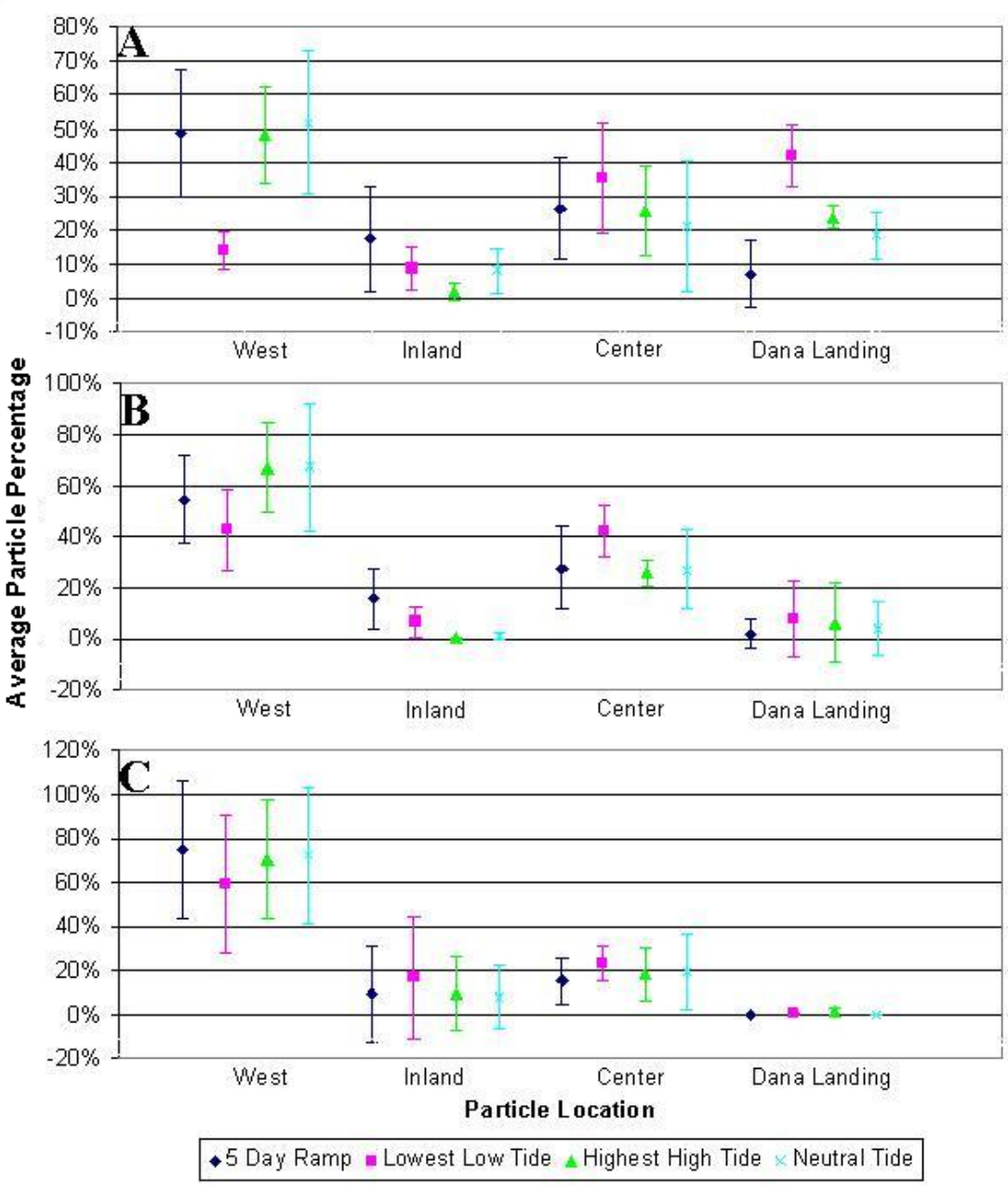

Figure 12. Effect of Release Time on Particles from Dana Landing: The average particle percentage reaching each section of Mission Bay due to release during different times in the tidal cycle and for no wind (A), varying wind (B) and westward wind (C) are shown. Average particle percentage is calculated by averaging the percentage of particles terminating in each section of Mission Bay which started in Dana Landing over all bottom stresses. Errors bars represent the standard deviation of average particle percentage and are one standard deviation above and below values.

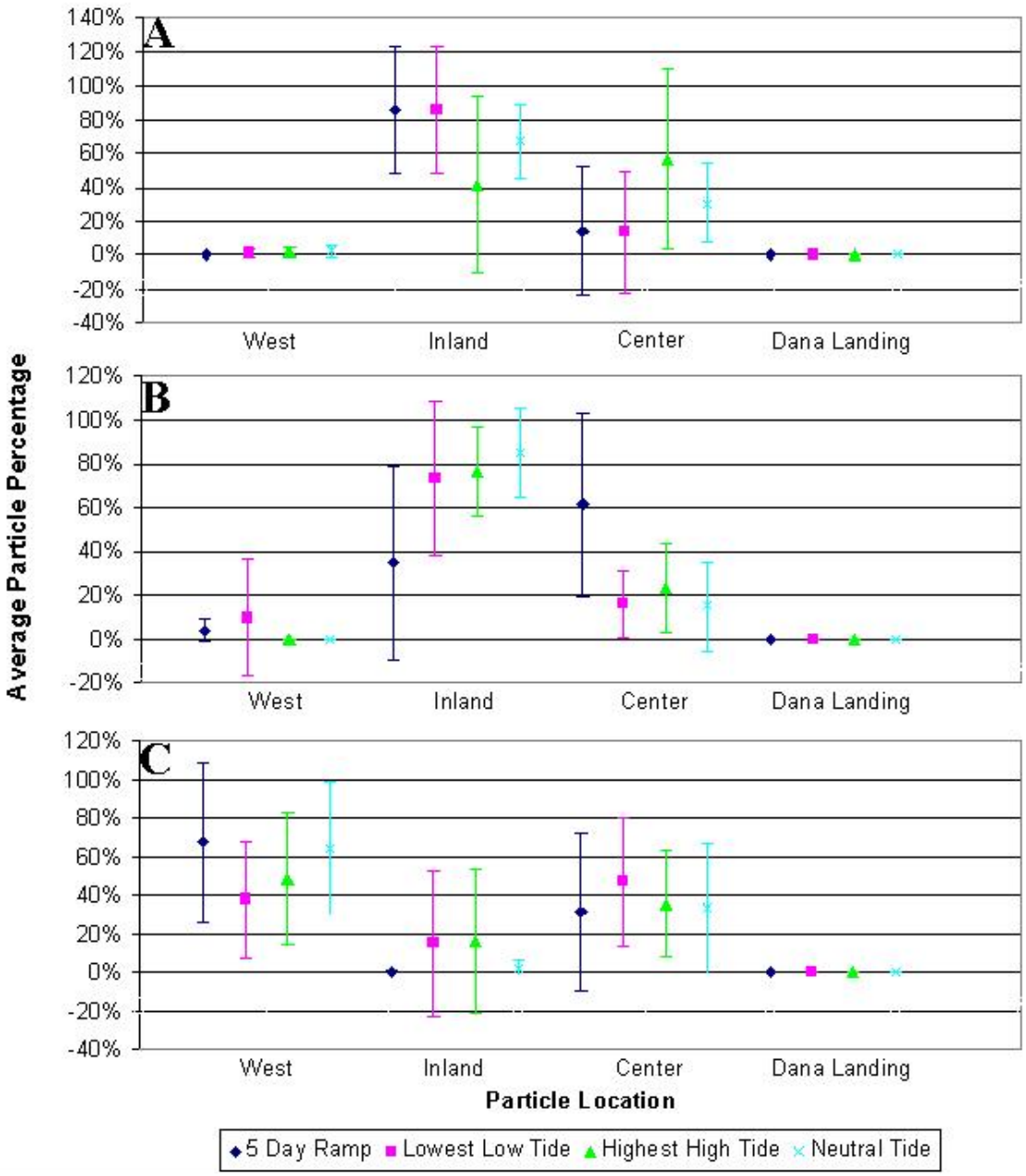

Figure 13. Effect of Release Time on Particle Trajectories from Marine Sanctuary: The average percentages of particles reaching each section of Mission Bay due to release during different times in the tidal cycle for no wind (A), varying wind (B), and westward wind (C) are plotted. No trends are seen for releases at particular release times. Error bars are one standard deviation above and below values.

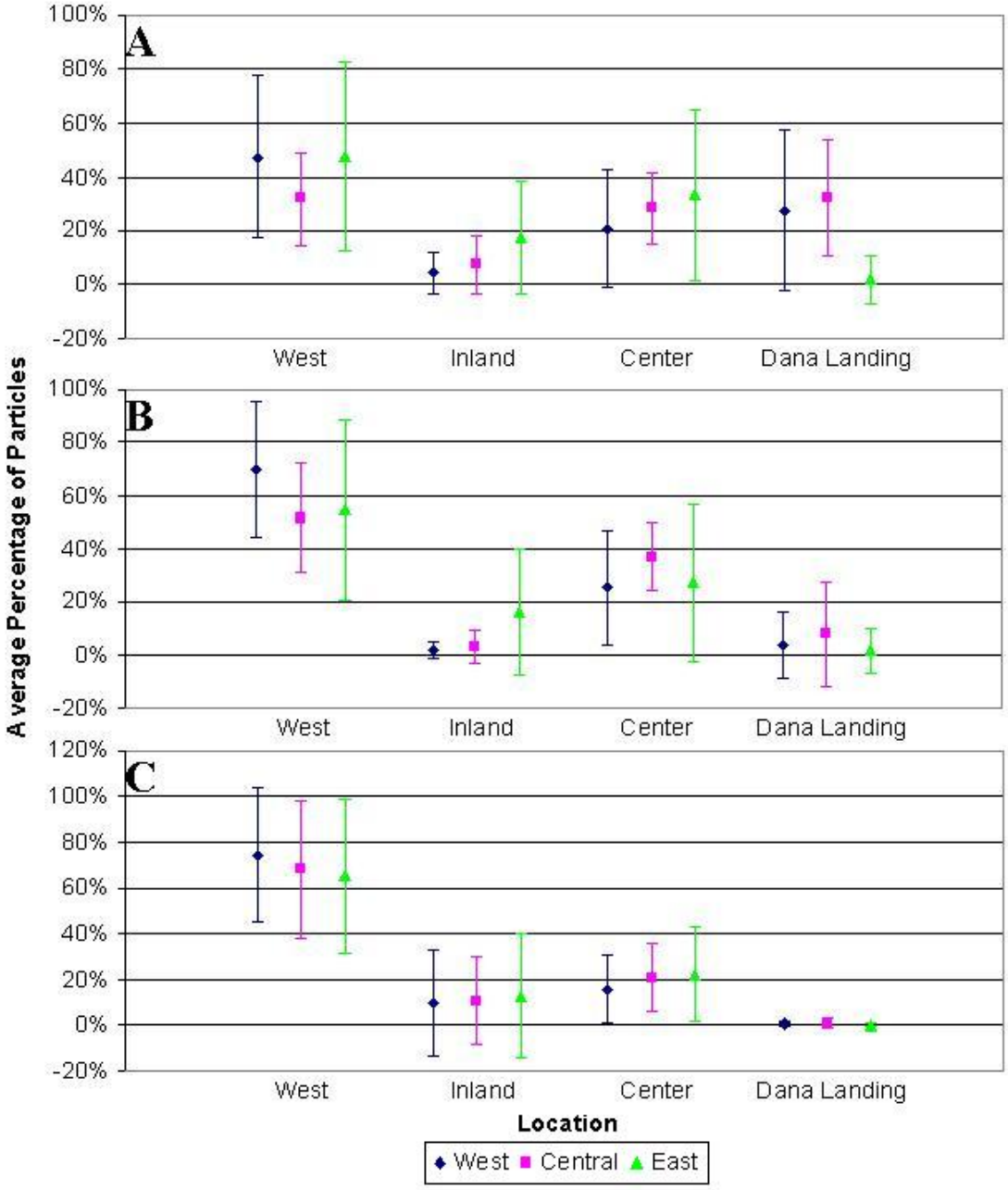

Figure 14. Effect of Releasing Particles from Different Parts of Dana Landing: The average percentage of particles released from each part of Dana Landing and their termination points are shown. Dana Landing is subdivided into three regions: west, central, and east. Three wind forcings are considered: no wind (A), varying wind (B), and westward wind (C). Markers represent which section of Dana Landing particles originate. Average percentages are computed by averaging termination locations over all release times and bottom stresses for each starting location. Error bars are one standard deviation above and below values.

Glossary

Roman Characters

A	Channel cross-sectional area
b_x, b_y	Baroclinic pressure gradients
B_x, B_y	Vertically-integrated baroclinic pressure gradients
C_D	Drag coefficient between air and ocean surface
C_u	Manning formula conversion unit
D_{slip}	Quadratic drag coefficient
D_x, D_y	Momentum dispersion
f	Coriolis parameter
g	Gravity
h	Bathymetric depth
H	Total water column thickness
$H\tau_{xx}$, $H\tau_{yx}$, $H\tau_{xy}$, $H\tau_{yy}$	Vertically-integrated lateral stress
k_{slip}	Slip boundary condition
n	Manning number
M_x, M_y	Vertically-integrated lateral stress gradients
$P(x,y,z,t)$	Time-averaged pressure
P_s	Atmospheric pressure at the sea surface
$Q_{discharge}$	Flow rate in Manning formula
Q_n	Outward flux per unit width normal to the boundary
Q_x, Q_y	x, y directed fluxes per unit width
R	Hydraulic radius
S	Hydraulic head loss.
t	Time
T	Integration time scale for separating turbulent and time-averaged quantities
$u(x,y,z,t)$, $v(x,y,z,t)$, $w(x,y,z,t)$	Time-averaged velocities in the x, y, and z directions
$u'(x,y,z,t)$, $v'(x,y,z,t)$, $w'(x,y,z,t)$	Departures of the instantaneous turbulent velocities from the time-averaged velocities
$U(x,t)$	Velocity used in Runge-Kutta 4
U, V	Depth-averaged velocities in the x and y directions
U_{wind}, V_{wind}	Zonal and meridional wind velocities

x , y	Horizontal coordinate direction
z	Vertical coordinate direction

Greek Characters

α	Effective Earth elasticity factor
Γ	Boundary of the computational domain
Δt	Time step between ADCIRC velocity outputs
ζ	Free surface elevation
η	Newtonian equilibrium potential
ν	Molecular viscosity
$\rho(x, y, z, t)$	Density of water
ρ_o	Reference density of water
ρ_{air}	Density of air
τ_o	Weighting factor in Generalized Wave Continuity Equation
τ_{bx} , τ_{by}	Bottom stress components
τ_{sx} , τ_{sy}	Imposed surface stresses
$\tau_{xx}(x, y, z, t)$, $\tau_{yx}(x, y, z, t)$, $\tau_{zx}(x, y, z, t)$, $\tau_{xy}(x, y, z, t)$, $\tau_{yy}(x, y, z, t)$, $\tau_{zy}(x, y, z, t)$	Combined viscous and turbulent Reynolds stresses
τ_{wind}	Wind stress
ϕ_j	Weighting function
X	Tidal generating potential
Ω	Horizontal computational domain

Work Cited

Barnes, H. H. 1967. Roughness characteristics of natural channels. *US Geological Survey Water Supply Paper 1849*. Pp. 1-10.

Becker, B. J., F. J. Fodrie, P. A. McMillan, L. A. Levin. 2005. Spatial and Temporal Variation in Trace Elemental Fingerprints of Mytilid Mussel Shells: A Precursor to Invertebrate Larval Tracking. *Limnology and Oceanography* 50(1): 48-61.

Cáceres-Martínez, J. and A. Figueras. 1997. The mussel, oyster, cockle, clam and pectinid fisheries in Spain. *NOAA Technical Report* NMFS 129:165-190.

Connor, J.J., and C.A. Brebia. 1976. Finite Element Techniques for Fluid Flow. Butterworth & Co. Ltd. Woburn, Massachusetts, USA. Pp. 233-257.

Cowen, R. K., and S. Sponaugle. 2009. Larval Dispersal and Marine Population Connectivity. *Annual Review of Marine Science* 2009 1: 443-466.

Cowen, R. K., G. Gawarkiewicz, J. Pineda, S. R. Thorrold, and F. E. Werner. 2007. Population Connectivity in Marine Systems An Overview. *Oceanography* 20(3): 14-21.

Crooks, J. A. 1998. Habitat alteration and community-level effects of an exotic mussel, Musculista senhousia. *Marine Ecology Progress Series* 162:137-152.

Crooks, J.A. 2002. Predators of the invasive mussel Musculista senhousia (Mollusca: Mytilidae). *Pacific Science* 56(1): 49-56.

Dexter, D.M. and J.A. Crooks. 2000. Benthic communities and the invasion of an exotic mussel in Mission Bay, San Diego: A long-term history. *Bulletin Southern California Academy of Science* 99(3): 128-146.

Dill, N. L. 2007. Hydrodynamic Modeling of a Hypothetical River Diversion Near Empire, Louisiana. Masters Thesis, Louisiana State University, Baton Rouge, LA, USA.

De Doncker L, Troch P, Verhoeven R, Bal K, Meire P. 2009. Determination of the Manning roughness coefficient influenced by vegetation in the river Aa and Biebrza River. *Environmental Fluid Mechanics* 9: 549-567.

Ebersole, B.A., J.J. Westerink, S. Bunya, J.C. Dietrich, and M.A. Cialone. 2009. Development of Storm Surge Which Led to Flooding in St. Bernard Polder during Hurricane Katrina. *Ocean Engineering* 37(1): 91-103.

Grahame, J. and G.M. Branch. 1985. Reproductive patterns of marine invertebrates. *Oceanography and Marine Biology: An Annual Review* 23: 373–398.

Gray, W.G. and D.R. Lynch. 1979. On the Control of Noise in Finite Element Tidal Computations: a semi-implicit approach. *Computers and Fluids* 7(1): 47-67.

Hench, J.L., R.A. Luettich, Jr., J.J. Westerink and N.W. Scheffner. 1995. ADCIRC: an advanced three-dimensional circulation model for shelves, coasts and estuaries, report 6: development of a tidal constituent data base for the Eastern North Pacific, Dredging Research Program Technical Report, U.S. Army Corps of Engineers Waterways Experiment Station, Vicksburg, MS.

Hicks, S. D. 2006. Understanding Tides. National Oceanic and Atmospheric Administration, National Ocean Service**,** Silver Springs, MD. Pp. 1-10

Hill, D.F. 2007. Tidal Modeling of Glacier Bay, Alaska - Methodology, Results, and Applications.

Kinnmark, I.P.E. 1986. The shallow water wave equations: formulations, analysis and application, Lecture notes in engineering vol. 15**,** Springer-Verlag, Berlin. Pp 1-26.

Largier, J. L., J. T. Hollibaugh, and S. V. Smith. 1997. Seasonally hypersaline estuaries in Mediterranean-climate regions. *Estuarine, Coast and Shelf Science* 45:789-797.

Levin, L.A. 1983. Drift tube studies of bay-ocean water exchange and implications for larval dispersal. *Estuaries* 6(4): 364-371.

Luettich, R.A., J.J. Westerink, and N.W. Scheffner. 1991. ADCIRC: an advanced three-dimensional circulation model for shelves, coasts and estuaries, Report 1: Theory and methodology of ADCIRC-2DDI and ADCRIC-3DL. Coastal Engineering Research Center, U.S. Army Engineers.

Luettich, R.A., Jr., J.L. Hench, C.D. Williams, B.O. Blanton, and F.E. Werner. 1998. Tidal circulation and larval transport through a barrier island inlet, Estuarine and Coastal Modeling V, M. Spaulding et al. [eds]. American Society of Civil Engineers. 849-863.

Luettich, R. A., J. L. Hench, C. W. Fulcher, F. E. Werner, B. O. Blanton, and J. H. Churchill. 1999. Barotropic tidal and wind-driven larval transport in the vicinity of a barrier island inlet. *Fisheries Oceanography* 8(suppl. 2):190–209.

Luettich, R.A., J.J. Westerink, and N.W. Scheffner. 2004. Formulation and Numerical Implementation of the 2D/3D ADCIRC Finite Element Model Version 44.XX.

Luettich, R.A., Westerink, J.J. and N.W. Scheffner. 2006. ADCIRC: A (PARALLEL) ADVANCED CIRCULATION MODEL FOR OCEANIC,COASTAL AND ESTUARINE WATERS.

Lynch, D.R. and W.G. Gray. 1979. A Wave Equation Model for Finite Element Tidal Computations. *Computer and Fluids* 7(3): 207-228.

MacDonald, K. B. 1969. Quantitative studies of salt marsh mollusc faunas from the North American Pacific coast. *Ecological Monographs* 39(1):33-59.

McQuaid, C. D. and T. E. Phillips. 2000. Limited wind-driven dispersal of intertidal mussel larvae: in situ evidence from the plankton and the spread of the invasive species Mytilus galloprovincialis in South Africa. *Marine Ecology Progressive Series* 201: 211–220.

Muccino, J. C. 1995. Formulation and Application of Data Assimilation Techniques in Finite Element Shallow Water Equation Modeling. Ph.D. Dissertation, University of Notre Dame, Notre Dame, IN, USA.

Newman, W.A., and R.R. McConnaughey. 1987. A tropical Eastern Pacific barnacle, Megabalanus coccopoma (Darwin), in Southern California, following El Niño 1982–83. *Pacific Science* 41:31–36.

Rasmussen, L. L., B. D. Cornuelle, L. A. Levin, J. L. Largier, and E. Di Lorenzo. 2009. Effects of small-scale features and local wind forcing on tracer dispersion and estimates of population connectivity in a regional scale circulation model, *Journal of Geophysical Research* 114: C01012, doi:10.1029/2008JC004777.

Suchanek, T. H. 1979. The Mytilus californianus community: Studies on the composition structure, organization, and dynamics of a mussel bed. Ph.D. Dissertation, University of Washington, Seattle, WA, USA.

Weidemann, A., R. Arnone, R. Parsons, R. Gould, and S. Ladner. 2004. Ocean Color Satellite Derived Products in Support of Diver and Special Forces Operations During Operation Iraqi Freedom. Report, Naval Research Lab, Stennis Space Center, MS.